2005

The critical surface tension of 316L stainless steel

Henry Bueno
San Jose State University

THE CRITICAL SURFACE TENSION OF 316L STAINLESS STEEL

A Thesis

Presented to

The Faculty of the Department of Materials Engineering

San Jose State University

In Partial Fulfillment

of the Requirements for the Degree

Master of Science

by

Henry Bueno

May 2005

INFORMATION TO USERS

The quality of this reproduction is dependent upon the quality of the copy submitted. Broken or indistinct print, colored or poor quality illustrations and photographs, print bleed-through, substandard margins, and improper alignment can adversely affect reproduction.

In the unlikely event that the author did not send a complete manuscript and there are missing pages, these will be noted. Also, if unauthorized copyright material had to be removed, a note will indicate the deletion.

ProQuest Information and Learning Company
300 North Zeeb Road
P.O. Box 1346
Ann Arbor, MI 48106-1346

APPROVED FOR THE DEPARTMENT OF CHEMICAL AND MATERIALS ENGINEERING

Guna Selvaduray

Dr. Guna Selvaduray

Dr. Sepehr Fariabi, Edwards Lifesciences

Dr. Manfred Cantow

APPROVED FOR THE UNIVERSITY

Abstract

THE CRITICAL SURFACE TENSION OF 316L STAINLESS STEEL

by Henry R. Bueno

Thrombogenicity (surface induced blood-clotting) is a major issue with metallic stent implant-devices. Although the exact causes for this are unclear, it is thought that several surface properties are responsible. In this study the critical surface tension of 316L stainless steel was investigated, as a function of surface treatments and plastic strain. The critical surface tension, which is related to the solid's surface tension, has been shown in previous work to correlate with the thrombogenicity of implant materials.

Using the Zisman technique to analyze contact angle data, obtained from sessile drop measurements, the critical surface tension was determined. It was found that the surface treatment consisting of electropolishing, followed by passivation for 30 minutes in 30% nitric acid, resulted in the only surface that lied within the previously established range of biocompatibility. Additionally, surface strain up to 30% did not result in a significant change to the critical surface tension.

Acknowledgments

I would like to acknowledge my wife Analia and daughter Ryana for their patience with me, as I spent the time in completing this work. In addition to their patience, their constant support helped me to find the energy to continue with and complete this work.

I would also like to acknowledge each of my committee members. First and foremost, I would like to thank Dr. Selvaduray for his never-ending persistence in ensuring that I never lost sight of the finish line. In addition to his excellent technical coaching and mentoring, his genuine sense of dedication towards my completion of this work made it impossible for me to do otherwise.

I would also like to thank Dr. Fariabi and Dr. Cantow for their technical guidance at all points along the way, as well as their constant willingness to discuss through any issues I encountered. Dr. Fariabi, in particular, was instrumental in helping to define the subject of this work.

Thanks also to the SJSU Chemistry Department for use of their AFM equipment, as well as to Pull-Bright Inc. (Fremont) for eletropolishing services.

Table of Contents

Table of Contents, continued

Table of Contents, continued

List of Tables

List of Tables, continued

List of Figures

List of Figures, continued

Chapter 1
Introduction

1.1 Artherosclerosis

Artherosclerosis has become a problem disease in today's society. It is estimated that 50 percent of all deaths in the United States and Western Europe can be attributed to atherosclerosis [1] - the buildup of cholesterol plaque in the arteries that constricts blood-flow. Artherosclerosis can affect all vessels of the arterial system, frequently resulting in long-term blockage (occlusion) of the artery. As early as 1912 the physician Alex Carrel recognized the potential to bolster weakened arteries in the human body through introduction of a tubular implant. Although his idea was innovative, his choice of materials - glass and aluminum - resulted in a low success rate in dog specimens [2].

Carrel's idea was not furthered until 1964 when Charles Dotter was able to achieve successful catheter insertion of intra-arterial scaffolds. However, early attempts at sliding plastic, coaxial tubes with gradually increasing diameter into blocked vessels were also unsuccessful. These early implants suffered from implant migration and, what continues to be problematic today, implant surface-induced blood-clotting (thrombosis) [3].

In 1978 the physician Andreas Gruntzig developed what would become the standard non-surgical treatment for atherosclerotic blockages; this procedure he called "percutaneous transluminal coronary angioplasty" (PCTA) or simply "angioplasty" [4]. In the angioplasty procedure a balloon at the tip of a catheter is inserted into the femoral

artery and then advanced along a guide wire until it is correctly positioned at the blockage site, where the balloon is then inflated - flattening the plaque against the arterial wall. This procedure is depicted in Figure 1.

Although angioplasty is less invasive than coronary-bypass surgery, which translates to less recuperation time and lower associated costs, there are two major problems with the procedure: vessel closure immediately following the procedure, and a re-growth of the plaque within the first 6 months after treatment - a process known as restenosis.

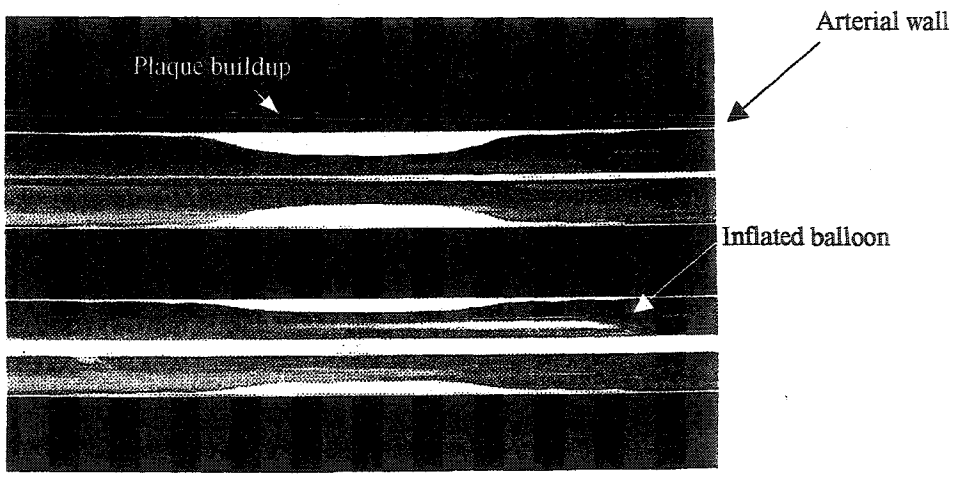

Figure 1. The angioplasty procedure: a) insertion of guide-wire into artery, and b) flattening of plaque against arterial wall [5].

Several years afterwards, in an attempt to address the shortcomings of Gruntzig's angioplasty procedure, Dotter applied the work he had developed two decades earlier.

This time however he began working with implants that consisted of uncoated wire coils made from the nickel-titanium alloy, Nitinol. The unique shape-memory properties of Nitinol allowed the coils to be inserted in a compacted form. Then, after flushing with warm saline solution (at a temperature of 60°C), the coil assumed its original shape [6]. This process of inserting tube-shaped implants directly into the artery would later become known as "stenting." Dotter had also previously laid the foundation for stent materials by establishing the relative biocompatibility of stainless steel coils, or stents, for this purpose [7]. The new materials, in addition to a reduced metal surface coverage, were found to encourage prompt incorporation of the stent into the artery's endothelial lining, thereby increasing the rates of long-term biocompatibility.

By 1987 there was clinical evidence to suggest that coronary stent implantations were successful for the treatment of the adverse effects associated with angioplasty [8,9]. Boosted by this clinical data, stenting has seen a soaring increase in usage and an increase in the diversity of applications. With stents now being placed in the peripheral and carotid arteries, in addition to the coronaries.

1.2 What is a Stent?

Endoluminal Arterial Stents, or simply "stents," have become one of the more important, and commonly used, implants in the field of interventional cardiology today. As a treatment for the negative side effects of the angioplasty procedure, namely sudden arterial collapse and re-growth of plaque following angioplasty (restenosis), these tube-

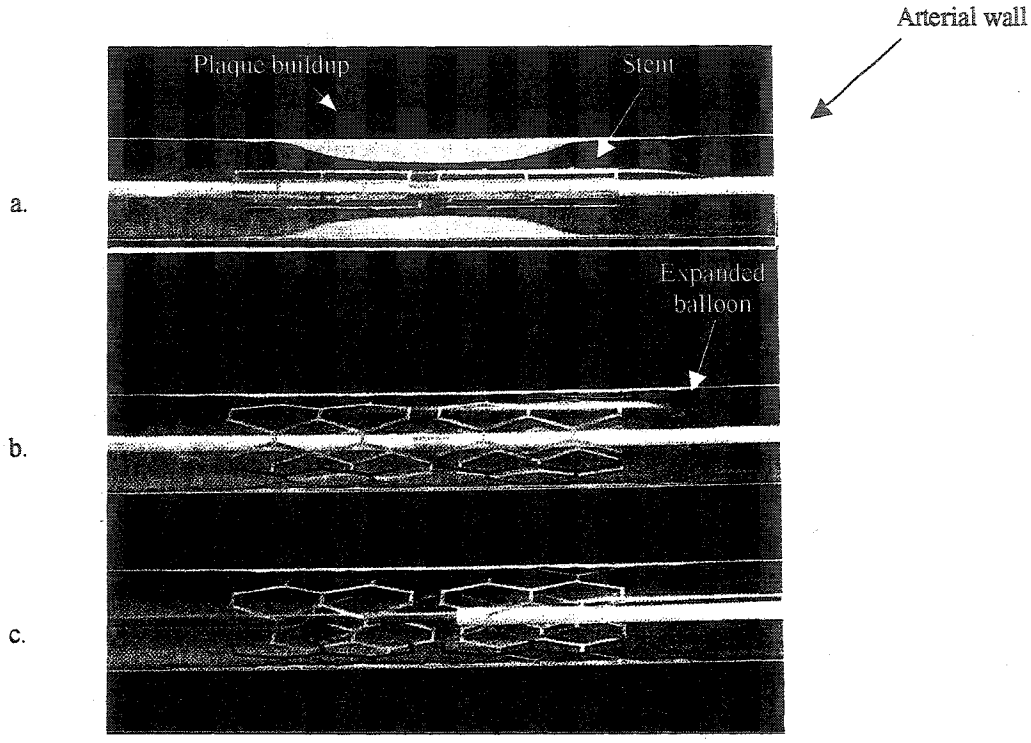

Figure 2. The stenting process: a) insertion of stent into blockage-site, b) balloon-expansion of stent, and c) removal of the stent delivery system [5].

The second requirement is that at the stent/blood interface the stent surface should be sufficiently un-reactive to the passing blood, in particular platelet cells, so as not to induce thrombosis. An effective stent is then a compromise between these two requirements. Stents composed of metallic materials, for reasons that remain unclear, are frequently found to have greater difficulty satisfying the second of the above requirements.

In addition to the strict biological requirements, stents also must possess sufficient mechanical and corrosion resistant properties. It is then not surprising that the list of

possible materials suitable for use in stents is relatively short. This list includes the low-carbon 316L stainless–steel alloy, the equi-atomic nickel-titanium alloy known as Nitinol, the nickel-cobalt alloy MP35N, certain Cobalt-Chromium alloys, and the pure metals Tantalum and Platinum. The material of choice for use in stents has been 316L stainless steel - with approximately 70% of all stents being fabricated from this material [10]. The relative ease of fabrication, wide-spread availability of raw materials from manufacturers, low cost, and good mechanical and biological properties are a few of the reasons that 316L is preferred to all other metals. However, not all aspects of 316L, especially with regards to biocompatibility, have been thoroughly investigated. This investigation will address an area regarding the surface characteristics of 316L stents that has not been researched previously.

1.3 Scope of Research

This study was undertaken to investigate in-vitro surface effects of 316L stainless steel, with respect to liquid interactions. The focus was on the specific factors that are known to alter the surface state of 316L stainless steel, and how these affect the reactivity of the implant surface in-vitro and therefore its relative propensity to induce thrombosis in-vivo.

The mechanism of stent-induced thrombosis discussed in this work refers to thrombosis that is initiated at the material/blood interface. This is differentiated from thrombus that initiates at the endothelial wall, which typically can result from damage to the endothelial lining during an incorrectly performed stenting procedure, or, from device

malfunction. This form of thrombosis can, for example, result from an over expansion of the stent, or, incorrect sizing of the stent to the vessel. This mechanism of thrombosis, in contrast to implant surface-induced thrombosis, is well characterized from a physiological perspective.

The experimental approach taken in this work has been to investigate two specific surface properties of the 316L surface; surface energy and surface roughness, thought to be the most important properties with respect to biological interaction. These surface properties were evaluated as a function of surface treatments and plastic deformation. The two processes described here, surface treatment and plastic deformation, are processes representative of typical stent preparation and usage, and will serve as the input variables for the study. The results, in particular the measured surface energy, were then correlated with previous in-vivo studies to predict the relative thrombogenicity of the surface. Relative thrombogenicity was based on the results of previous researchers.

Chapter 2 contains a discussion of the elements of the biomaterial surface that are thought to be important in biological interactions, focusing on surface energy as a determinant of implant reactivity and long-term biocompatibility. Also contained in Chapter 2 are previous studies of the relationship between surface energy of biological implant surfaces and their biological interactions, both in-vitro and in-vivo. The research objectives of this work are presented in Chapter 3. The experimental approach that was used to determine surface energy and roughness, as well as the measured physical properties of the 316L test specimens that were used here are described in Chapter 4. The results of the surface energy and surface roughness measurements that were

conducted are presented in Chapter 5, while a discussion of the results and their significance in predicting relative thrombogenicity are given in Chapter 6. Finally, the conclusions that were drawn from this study are given in Chapter 7.

Chapter 2

Metallic Implants and Surface Tension

2.1 Factors That Affect Long-Term Stent Performance

Stent research has become a multi-disciplinary effort, encompassing the fields of medicine, materials science, surface chemistry, and mechanical engineering. In Table 1 is summarized the current areas of stent research and the scientific areas with which they are associated.

Table 1. Areas of Stent Research

Research Issue	Field(s) of Specialization	Region of stent involved
Thrombosis	Biological / Materials Science	Surface
Restenosis	Biological / Materials Science	Surface
Corrosion	Chemical / Materials Science	Surface
Strength/Ductility	Mechanical/Materials Science	Bulk
Design/Geometry	Mechanical Engineering (FMEA)	Bulk

The following criteria must be satisfied for metallic biomaterials to function effectively: (a) The bulk mechanical properties must be sufficient for the implant to meet its intended biological purpose, in particular yield strength and overall radial (hoop)

strength of the stent, (b) the material must not corrode in the body, potentially releasing toxic metallic ions into the bloodstream, and (c) the material must exhibit sufficient biocompatibility with the region of the body that it contacts.

For 316L stainless steel the adequacy of the mechanical and corrosion-resistance properties have already been established, and optimized, for in-vivo conditions through either heat or surface treatment [11]. However, the adverse clinical outcomes of restenosis and thrombosis still persist. Restenosis rates for 316L stents have been estimated at 20% to 40% [12]. Since restenosis is a slowly developing process, typically taking several months before an intervention is required, it can be monitored via angiograms and remedied by performing additional in-stent balloon angioplasty (PCTA) if necessary. Acute thrombosis is a much faster process, usually taking place within 24 hours after implantation, which makes detection by the physician and additional intervention more difficult. Although it is still unclear whether the problem of restenosis is an entirely surface-related phenomenon or not, the issue of stent thrombosis has been firmly established as being dependent on the surface material and condition. As a result, any process that alters the material's surface characteristics can then affect the relative thrombogenicity of the implant device. The rapid time frame that thrombogenicity operates in, as well as the immediate health risks, gives an added significance to elimination, or at least minimization, of this problem.

2.2 Thrombogenicity

As successful as stents are in bolstering weakened blood vessels they are not without their disadvantages. One of the biggest problems associated with stainless-steel stents is their ability to consistently induce surface blood clotting [13-15]. Known as thrombogenicity, this negative consequence of the stent implant has been found to increase quickly for arteries of decreasing diameter (< 2.0 mm), or in regions of reduced blood-flow. This has led to research into coating metallic stents with either passive layers of noble metals such as gold (Boston Scientific), diffusion-barriers such as silicon-carbide (Tensum stent) and amorphous carbon (Diamond AS stent), or drugs, to counteract thrombosis and restenosis (e.g., Johnson & Johnson's use of heparin coating). Efforts are underway to minimize the effects of thrombogenicity, and restenosis, by coupling active drugs via polymeric materials that would allow elution of the drug into the bloodstream (e.g., Johnson & Johnson's Cypher stent). However, these processes are still unproven in-vivo; questions still remain about the adhesion and uniformity of these coatings after stent-deformation, effects of long-term exposure to blood, as well as drug dosage and stability. Currently, 316L stainless steel stents undergo the same standard surface treatments that are performed on the low-carbon stainless steels used in the gas-delivery and food-service industries. These treatments, designed mainly for improvement in corrosion resistance, have been found to result in a reduction of stent thrombosis, although the mechanisms for this improved biological behavior is not entirely understood.

2.2.1 Mechanism of Arterial Thrombosis

The process of arterial thrombosis is characterized by a stimulation of platelet-cell adhesion and aggregation to a surface, which then, through a complex series of biochemical reactions, results in the formation of an expanding fibrin clot [16].

The exact reasons for why a particular foreign surface will stimulate platelet adhesion, while another may not, have not been clearly identified; however, the results are clear. In some instances, growth of the resulting clot will go unchecked until the blood vessel becomes completely occluded, at which point a heart attack is the probable outcome. In other instances, the clot breaks free of the surface and travels through the blood stream until it forms a blockage in another part of the body (embolization). This is particularly dangerous as stenting of the carotid artery, located within the brain, becomes increasingly popular. These events may also result in a heart attack, or stroke.

The issue of thrombogenicity has plagued stents since their usage began in the mid-1980s. Early clinical trials showed thrombosis rates in the range of 30-40%. By 1991 the rate decreased to approximately 20% due to better design and processing, and by 1994 the introduction of treatment regimens consisting of strong anti-platelet drugs, such as heparin, lowered rates to as low as 3.5% [17]. However, the major disadvantage embodied in the use of anti-platelet drugs is their inhibition of the natural healing response of the body - an undesirable outcome considering that stents are typically inserted through an incision in the femoral artery. It is then desirable to search for methods to render current stent materials less thrombogenic, and therefore less dependant

on drugs. A thrombosis-resistant surface would also have positive implications for the stenting of small-diameter arteries (< 2.5mm), where thrombosis is more likely.

2.3 The Biomaterial Surface in Stent Thrombogenesis

The most important factor in determining thrombogenicity in blood-contacting implants, such as a stent, is the condition of the surface. As such, much of the literature on the biocompatibility of cardiovascular implants has focused on ways to minimize thrombogenicity through investigation of one or more surface properties. As yet there is no definitive list of which surface properties contribute to thrombogenicity – much less what values, or range of values, these properties should assume. Nonetheless, a summary of some of the surface properties thought to be important to thrombogenicity is listed in Table 2.

One particular area of thrombosis research has focused on correlating the relative thrombogenicity of biological implants to their surface energy, or surface tension. Surface tension results from the fact that atoms at the surface of a material have a number of unsatisfied bonds, compared to atoms in the bulk. The energy associated with these unsatisfied bonds is what then gives rise to surface tension. The surface tension of the (solid) implant material, the surface tension of the (liquid) blood, and the resulting interfacial tension that occurs after implantation, all determine the extent to which blood "wets" the implant surface.

Table 2. Surface Characteristics of Implants and their Effect on Thrombogenicity

Surface Property	Effect on Thrombogenicity	Reference
Surface Charge (Potential)	unclear	18-22
Surface Texture (Roughness)	Increases with roughness	18-22
Surface Free Energy (Tension)	Varies from regions of low to high thrombogenicity	18-21
Surface Composition (Oxide chemistry)	unclear	18-20
Grain Structure, Size, or Orientation	unknown	unknown

The degree of wettability of an implant by blood has been found to have significant effects on the resulting adhesion between the surface of the implant and the biological components present in the blood-stream [23-25]. The surface energy of a stent implant is then an important factor in long-term biocompatibility. This solid surface energy is quantified as its "specific surface free energy," or equivalently, its surface tension (γ).

2.4 Surface Tension of Solids and Liquids

Solids and liquids alike have tension (energy) associated with their surfaces. Young first described the relationship between a liquid with surface tension, γ_L, and a solid with surface tension, γ_S, in the early 1800's. He described the interaction between the liquid and solid surface by way of the contact angle (θ_C). The contact angle was defined as the angle measured from the solid surface to the tangent of the resulting liquid

droplet (when drawn from the interface of the liquid, solid, vapor phase). Illustrations of possible θ_C conditions are shown in Figure 3.

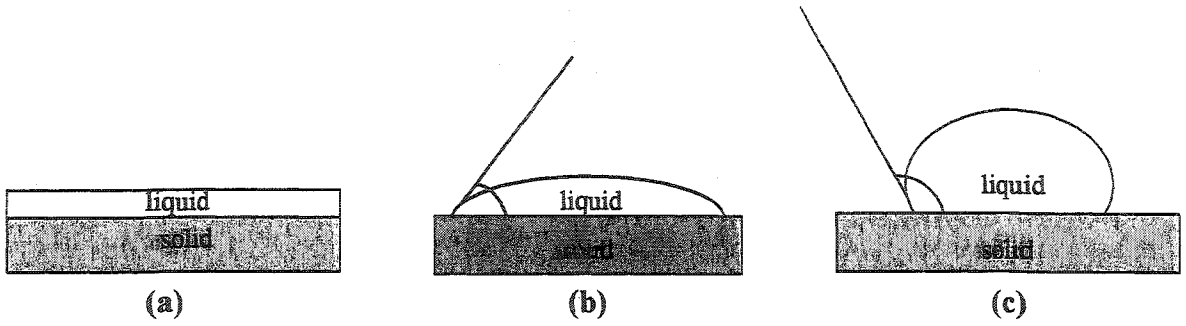

Figure 3. Possible variations of Young's contact angle showing a) $\theta_c = 0$ (complete wetting), b) $0 < \theta_c < 90$ (wetting), and c) $\theta_c > 90$ (partial wetting)

The Young equation that describes the shape of the contact angle is analytically expressed in the form of Equation 1:

$$\cos \theta_c = (\gamma_S - \gamma_{SL}) / \gamma_L \qquad \text{Equation 1}$$

where γ_{SL} is the interfacial tension at the liquid/solid interface.

Dupre later defined the work of adhesion, ΔG_{SL}, between a solid surface and a liquid as:

$$\Delta G_{SL} = \gamma_{SL} - \gamma_S - \gamma_L \qquad \text{Equation 2}$$

Insertion of Equation (2) into Equation (1) yields the well-known Young-Dupre equation:

$$-\Delta G_{SL} = \gamma_L (1 + \cos \theta_c) \qquad \text{Equation 3}$$

The Young-Dupre equation illustrates the nature of the sessile contact angle as a force balance, as shown in Figure 4. The $\cos \theta_c$ term is a measure of the equilibrium between the cohesive forces of the liquid droplet (γ_L^{total}) and the adhesion force at the liquid/solid interface ($-\Delta G_{SL}^{total}$).

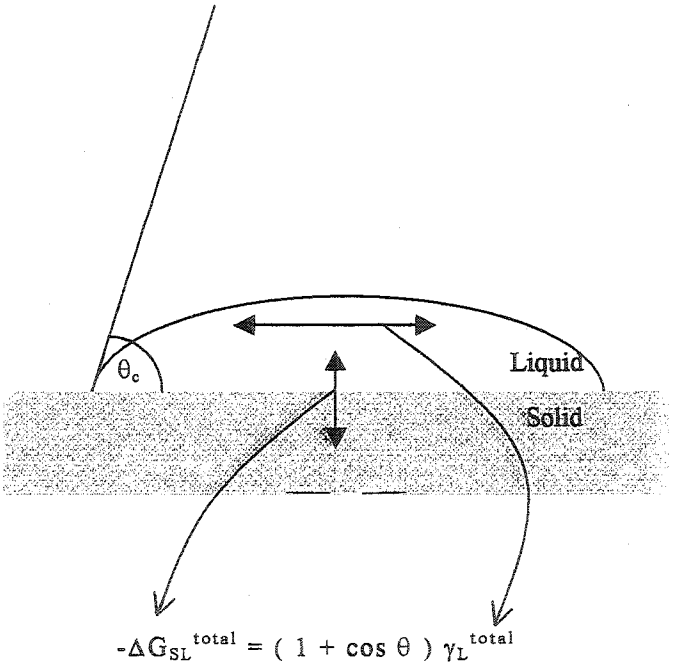

Figure 4. The sessile contact angle as a force balance [26].

The total surface tension of a solid (γ_S) has since been shown to be an additive quantity composed mainly of two dominant components: 1) a component due solely to

dispersive (Van der Waals) interactions, γ_S^d, and 2) a component arising from any polar (hydrogen-bonding) interactions, γ_S^p. The total surface tension of the solid can then be written as,

$$\gamma_S^{total} = \gamma_S^d + \gamma_S^p \qquad \text{Equation 4}$$

Currently, there exist contact-angle measurement methods to determine γ_S^{total} from 2 distinct liquids [27], or 3 distinct liquids [26], using Equations 3 and 4 as a basis for the derivation. However, there does not exist a consensus, among researchers in the field, as to which method yields greater accuracy. Since the Young Equation (Equation 1) does contain 3 unknown terms (γ_S, γ_L, and γ_{SL}), it is reasonable to require at least 3 unique contact angles for their determination. As yet, the literature has not reflected correlations of γ_S^{total} with in-vivo biological interaction.

2.4.1 The "Critical" Surface Tension

An alternative approach to estimate the surface tension of a solid was proposed by Fox and Zisman [28,29]. The Zisman approach is based on the empirical observation that the cosine of the wetting angle ($\cos \theta_c$) is a linear function of the corresponding liquid surface tension (γ_L) for liquids of the same chemical family (e.g., the alkane family of liquids). The proposed linear function is,

$$\cos \theta_c = 1 - b\ (\gamma_L - \gamma_{crit}) \qquad \text{Equation 5}$$

where b is a unitless constant usually in the range of 0.03 – 0.04. Each linear function, representing a particular solid surface, extrapolates to $\theta_C = 0$ ($\cos \theta_c = 1$) at a certain value, which Zisman defined as the "critical" surface tension (γ_{crit}). This value is "critical" in the sense that a liquid that has a surface tension equal to, or less than, this value will completely wet and spread spontaneously on that surface. This parameter, although not necessarily equal to, is conceptually related to the specific surface free energy of a material. In Figure 5 is shown a graphical description of the Zisman approach used to determine γ_{crit} values.

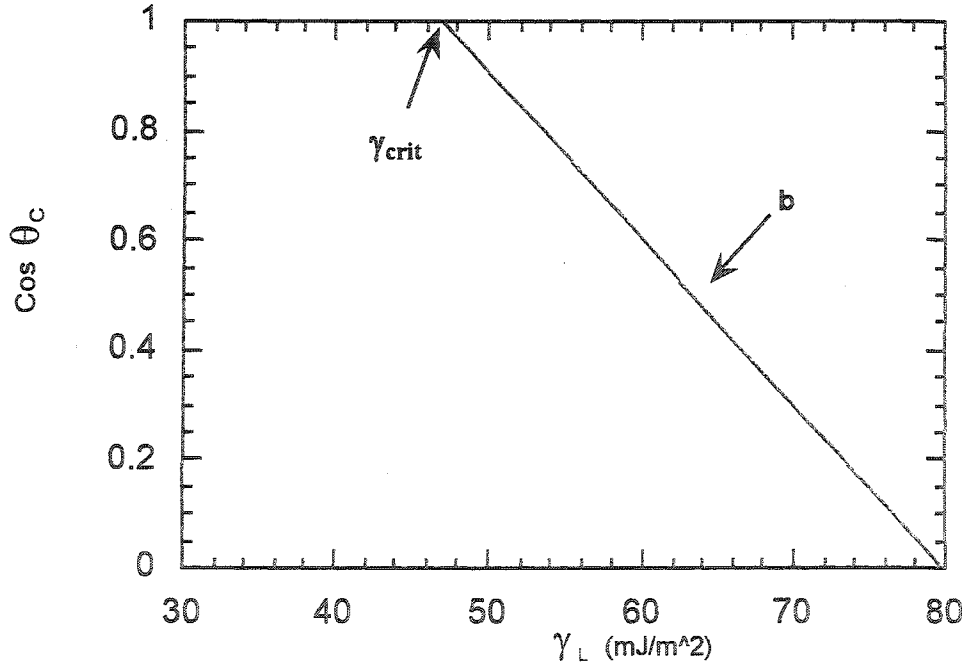

Figure 5. A graphical illustration of the Zisman technique, used to determine the critical surface tension (γ_{crit}) of a solid.

For a liquid that has only a dispersive component ($\gamma_L^{total} = \gamma_L^d$), interacting with a purely apolar surface ($\gamma_S^p = 0$), the Young-Dupre equation can be written as [26,30],

$$(1 + \cos \theta_c) \gamma_L = 2 [\gamma_S^d \gamma_L^d]^{0.5} \quad (6)$$

Rearranging gives,

$$\cos \theta_c = \{[2 (\gamma_S^d \gamma_L^d)^{0.5}] / \gamma_L\} - 1 \quad (7)$$

At complete wetting $\cos \theta_c = 1$. Therefore,

$$[(\gamma_S^d \gamma_L^d)^{0.5}] / \gamma_L = 1 \quad (8)$$

If test-liquids that contain only dispersive components ($\gamma_L = \gamma_L^d$) are used. Equation (7) then reduces to,

$$[\gamma_S^d / \gamma_L] = 1 \quad (9)$$

and at complete wetting, since $\cos \theta_c = 1$, $\gamma_L = \gamma_{crit} = \gamma_S^d$. Therefore, for the specific case of non-polar test liquids on a non-polar surface the critical surface tension is identical to the solid surface tension, i.e., $\gamma_{crit} = \gamma_S^{total}$. All other cases will result in γ_S being different,

typically larger, than γ_{crit}. A comparison between the measured critical surface tension and solid surface tension for materials commonly used in the human body is provided in Table 3. Teflon is a known apolar surface; therefore its γ_{crit} and γ_S values are very similar. In contrast, the titanium-oxide layer that forms on titanium implants is thought to be a polar surface, and therefore its γ_S value is larger than its measured γ_{crit} value.

Table 3. Surface Tension Values of Common Biomaterials.

Material	**Typical Use in the Body**	**γ_{crit} (mJ/m^2)**	**γ_S (mJ/m^2)**	**References**
PTFE (Teflon)	Synthetic arterial grafts	18.5-22.0	17.9	28, 29, 31 (γ_{crit}) 26 (γ_S)
Nylon 6,6	Synthetic arterial grafts	34.9	40.7	From data in 26 (γ_{crit}) 27 (γ_S)
Titanium (un-treated)	Bone-contacting support	37.6	43.0	31, 32
Titanium (passivated)	Bone-contacting support	40.9	43.5	31, 32

2.5 Correlation of Implant Surface Tension with Thrombogenicity

Baier has established a correlation between the critical surface tension of implant surfaces and their thrombogenicity in-vivo [33]. Baier's methodology consisted of first measuring the γ_{crit} values of many materials using the Zisman technique, followed by

implantation in animals to various time points, then retrieval of the material and visual examination of the material surface and surrounding tissue. His results, presented in Figure 6, show a variation in the level of biological interaction as a function of the implant's critical surface tension. In particular, surfaces exhibiting γ_{crit} values greater than approximately 40 mJ/m^2 have a rapidly increasing level of interaction. With respect to the lower extreme of the curve, the lack of availability of materials with extremely low solid surface tension inhibited investigation of biological response in this region. Of importance to this study is the narrow region between 20-30 mJ/m^2, and particularly the minima that occurs at approximately 25 mJ/m^2, in which Baier identified as the region

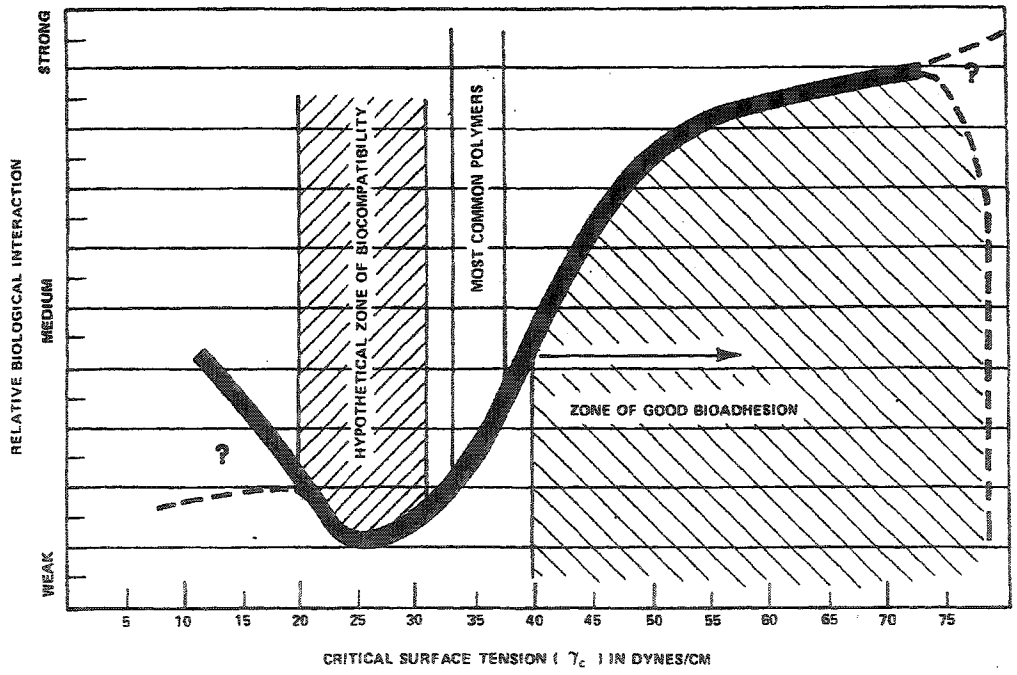

Figure 6. Effect of an implants critical surface tension on its biological interaction with the body [33].

where the least amount of thrombosis was observed and subsequently concluded that reactivity between implant and blood was at a minimum. For stents, these findings translate to a minimization in interaction between the stent and blood-flow, or alternatively, a reduction in thrombogenicity. Additionally, Baier observed that implants that had not formed thrombus had instead quickly formed a thin protein layer that had apparently passivated the surface from attachment of platelet cells. Unfortunately, a thorough characterization of the material surface was lacking; information on surface chemistry and roughness was not reported. Regardless, Baier's results provide a means of predicting an implant's relative performance, in-vivo, without requiring animal experimentation.

The data of Coleman et al. [34] also demonstrate a similar result. These data indicate a trend of faster thrombus formation with increasing solid surface tension, γ_S. Coleman's initial objective was to investigate two hypotheses regarding implant thrombogenicity: the minimum interfacial free energy hypothesis and the optimum polar/apolar ratio hypothesis. The former states that as γ_{SL} approaches zero so should the driving force for biological interaction (adsorption of blood components onto the surface), while the latter states that there is an optimal ratio of $\gamma_S{}^p$ to $\gamma_S{}^d$ that results in the formation of an implant-protecting layer of proteins. Using a captive bubble underwater contact angle technique to determine the surface tensions (γ_S) of a series of materials, followed by whole blood clotting time (WBCT) measurements on the same surfaces, Coleman concluded that neither hypothesis could explain his experimental findings. However, his original WBCT data, when plotted as a function of the total solid

surface tension ($\gamma_S{}^T = \gamma_S{}^d + \gamma_S{}^p$) does demonstrate a strong inverse correlation of thrombus formation with solid surface tension, as shown in Figure 7. Although still plausible from a thermodynamic perspective, these results were obtained in conditions of significantly reduced blood-flow and are therefore not necessarily representative of in-vivo conditions. Surface characteristics of Coleman's test surfaces, such as roughness and surface impurities that could affect surface tension, were not investigated.

Van Oss [26] measured the interfacial energies between human plasma proteins and several materials in water, and showed that the "attractive" energy between proteins and surfaces is the greatest for materials that have lower solid surface tension (γ_S in the range of 30-33 mJ/m^2). To explain the apparent contradiction with Baier's results, Van

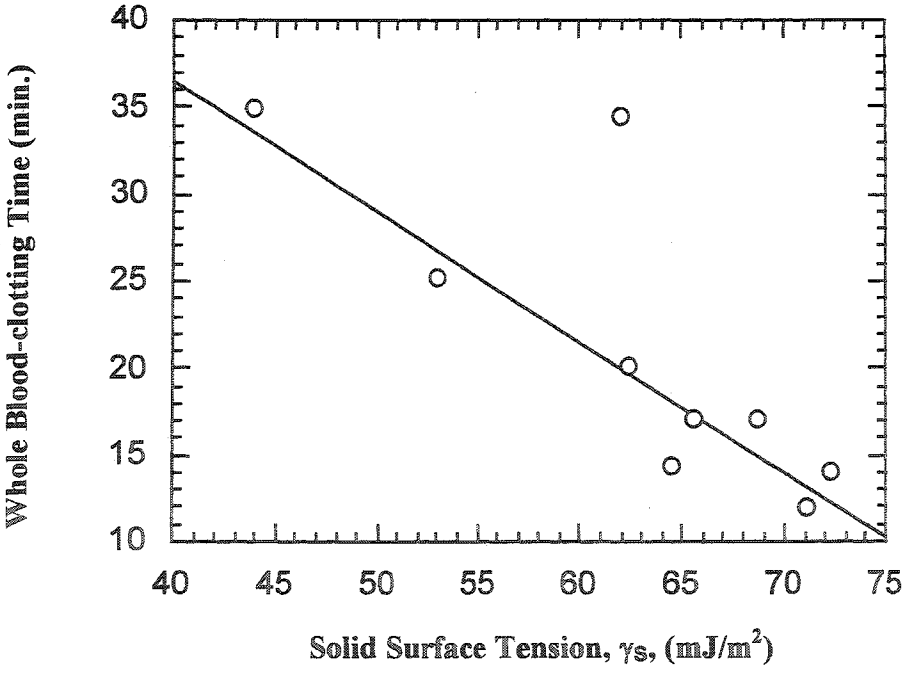

Figure 7. The effect of solid surface tension on the whole blood-clotting time of rabbits. Re-plotted with data from [34].

Oss has proposed that low to medium energy surfaces actually exhibit maximum attraction toward some blood components, such as cells and proteins, and since proteins (2-10 nm) are much smaller than platelet cells (2-4 μm) they are quickly attracted and bound to the implant surface. This layer of proteins then serves to passivate the surface within seconds against platelet aggregation. In contrast, high-energy surfaces experimentally exhibit lower degrees of attraction and therefore do not form a protective protein-layer – leading to exposure of the bare implant surface to arriving platelets, and subsequent thrombosis, a process illustrated in Figure 8.

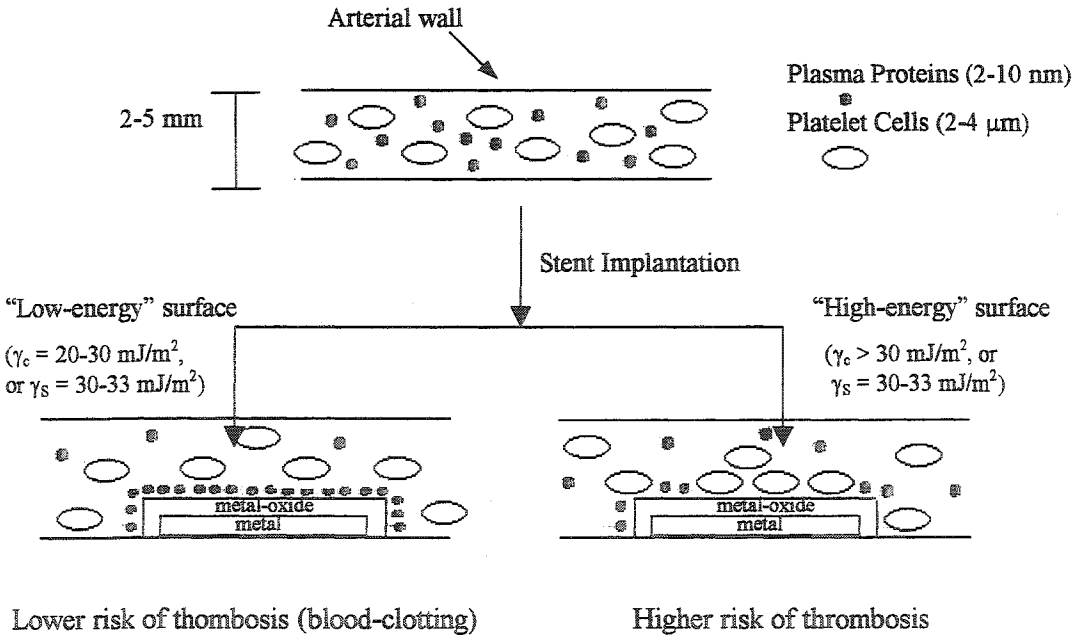

Figure 8. Illustration of the events immediately following stent implantation, and the significance of surface tension on long-term stent biocompatibility.

The implication for biomaterials is that in order to minimize thrombogenicity, through formation of a protective layer of proteins, the implant surface tension should have a γ_{crit} in the range of 20 –30 mJ/m^2 or, alternatively, a γ_S value in the range of 30-33 mJ/m^2. The surprising result is that the region of biocompatibility that Baier established, as shown in Figure 6 does not result from the surface becoming more inert, but rather from a surface that is most reactive selectively towards plasma proteins. The implication of this finding, from a materials design perspective, is that generally an increase in long-term biocompatibility can be expected when using biomaterials consisting of relatively lower surface tension, although other surface properties, interactions, and procedural effects may ultimately contribute to long-term biocompatibility as well.

2.6 Factors that Affect the Surface Tension of a Solid

Since surface tension is dependent on the state of the surface, anything that changes the nature of the surface is likely to result in changes in the surface tension. Surface characteristics such as surface texture, oxide composition and thickness, grain structure, as well as crystallographic orientation will in principle contribute to the total surface tension of a solid. Curvatures of the surface, as seen in tubing for example, also have been shown to influence the surface energy of 316L stainless steel [35].

In addition to inherent features associated with the surface, there are also external processes that can affect surface tension. Deformations of the surface, whether through tensile elongation or cold-rolling, will result in re-arrangement of atomic bonds and

changes in defect densities, which have been shown to also affect the surface tension in metals [36]. The issue of surface deformation is particularly relevant to stents because the stent implantation process requires a permanent (plastic), non-uniform, deformation of the stent.

Other external processes that affect solid surface tension are the processing steps needed to prepare a stent for implantation. It would be highly inadvisable to implant a stent that had not undergone any surface treatments, since the laser-cutting process used to fabricate stents results in a charred, jagged, surface that is prone to thrombogenicity. 316L stainless steel undergoes surface treatments, such as electropolishing and passivation, which are intended to enhance surface uniformity and improve the corrosion resistance of the material. However, it is not currently known how, or why, these treatments can affect biological interactions, such as thrombogenicity.

2.6.1 Effect of Surface Roughness on the Contact Angle

Since the surface tension of a solid has been known to change with surface roughness, the topography of the surface is an important variable that requires quantification whenever a wetting-angle approach is taken to characterizing a given surface. In light of constantly improving methods to modify surfaces, such as electropolishing and plasma techniques, it is important to know the state or nature of the surface from which the experimental measurements were derived, and more importantly for the materials engineer, what the relationship is between these variables.

R. Wenzel was the first to propose a quantitative relationship between surface roughness and the wetting-angle of a solid [37]. The Wenzel equation,

$$\cos \theta_{c,rough} = r \cos \theta_{c,true} \qquad \text{Equation 6}$$

relates the true contact angle to the measured contact angle by way of a unit-less variable defined as the "roughness factor (r)." The roughness factor is defined as the ratio between the actual surface area to the geometric (projected) surface area, and is an experimentally derived parameter. As a surface becomes increasingly rough, the peaks and valleys of that surface will contribute to an increased surface area. This roughness parameter amounts to the ratio between the actual 3-dimensional to the projected 2 dimensional surface areas. The r-value is experimentally derived from Atomic Force Microscopy (AFM) measurement. The statistical software packages of an AFM will typically calculate both actual and projected surface areas, and r-values can then be determined as the ratio of the actual to projected areas [32].

As predicted by Equation 6 an increase in the roughness of a surface will result in a decrease in the contact angle, for angles less than 90 degrees, which is typically observed in experiment.

Chapter 3
Research Objectives

3.1 Objectives

This study had two primary objectives. The first was to determine the effects of commonly implemented surface treatments on the critical surface tension of 316L stainless steel. Currently, it is not clear if and how the standard manufacturing processes used to fabricate 316L stent devices alter the surface tension (energy), and therefore the relative thrombogenicity, of the material surface. Surface treatments that include electropolishing and passivation are typically performed on chromium-bearing alloys, such as 316L, to increase corrosion-resistance. However, there are no current explanations as to why these same surface treatments result in better biocompatibility. This study was undertaken to investigate whether the improved biocompatibility of 316L, which results from surface treatments employed in the manufacturing process, can be related to surface tension effects. This was accomplished by measuring the critical surface tension of 316L in both the treated, and untreated, states. Then, correlating these experimental γ_{crit} values to the model already established, as shown in Figure 6, to predict relative thrombogenicity in-vivo.

The second objective was to determine the effects of plastic-strain on the γ_{crit} of 316L. This input variable was chosen because a unique feature of expandable stents is its requirement to be plastically deformed to over twice its radius upon implantation. However, a stent is typically designed to undergo non-uniform expansion, which means

that some areas of the stent will remain in an unstrained state, while other areas may experience strain levels of up to 30%. Since surface tension (energy) is thermodynamically predicted to increase with increasing surface strain the stent expansion process may result in the high-strain areas of the stent being prone to greater thrombogenicity than the unstrained portions. Measuring the critical surface tension of 316L that was plastically strained to levels of 15% and 30%, then comparing these values to the unstrained state tested this hypothesis.

As a secondary objective, the effects of surface treatment and strain on the surface topography (roughness) were also characterized. This additional surface characteristic was investigated because surface roughness is known to have an effect on the wetting characteristics of a particular surface. Therefore, any changes in surface tension for a given surface was then correlated with its topography to determine if roughness was a contributor to observed changes in surface tension.

Chapter 4

Methodology

4.1 Introduction

As was discussed in Chapter 3, the effects of surface treatments on critical surface tension were determined. The determination of this relationship required the choice of a relevant series of surface treatments. The choice of treatments was based on reproducing the exact processing steps that are encountered by a typical 316L stent. These steps would include,

1) Smoothing of the surface following the laser cutting of the stent design from raw hypotubing (tubing of diameters less than 5mm.). This is accomplished through use of an electropolishing treatment, where the stent is submerged in an electrolytic bath and current is passed through – preferentially removing material from the high and low points of the surface. The result is a surface with a mirror-like appearance.
2) Passivation steps to enhance surface-oxide uniformity. The current minimum requirement for preparing a low-carbon steel surface for implantation, as outlined in ASTM F-86 [38], is to passivate the surface through immersion for 30 minutes in a solution of 30%-60% nitric acid, at room temperature.
3) Finally, the entire stent and delivery system would be sterilized together, typically using ethylene-oxide gas (EtO) as a sterilizing agent. The requirements here are that the sterilizing process is low temperature, so as not to degrade the polymer materials

frequently used in stent delivery systems; and to ensure that the sterilizing agents not leave residual traces afterwards.

In order to test the effects of plastic deformation on the critical surface tension, test specimens were plastically elongated. Metals, upon straining, experience first an elastic deformation, the extent of which is illustrated by the point ε_Y in Figure 9. This elastic strain is recovered immediately upon unloading of the material. However, straining beyond the elastic region causes plastic deformation to begin, resulting in permanent deformation of the metal.

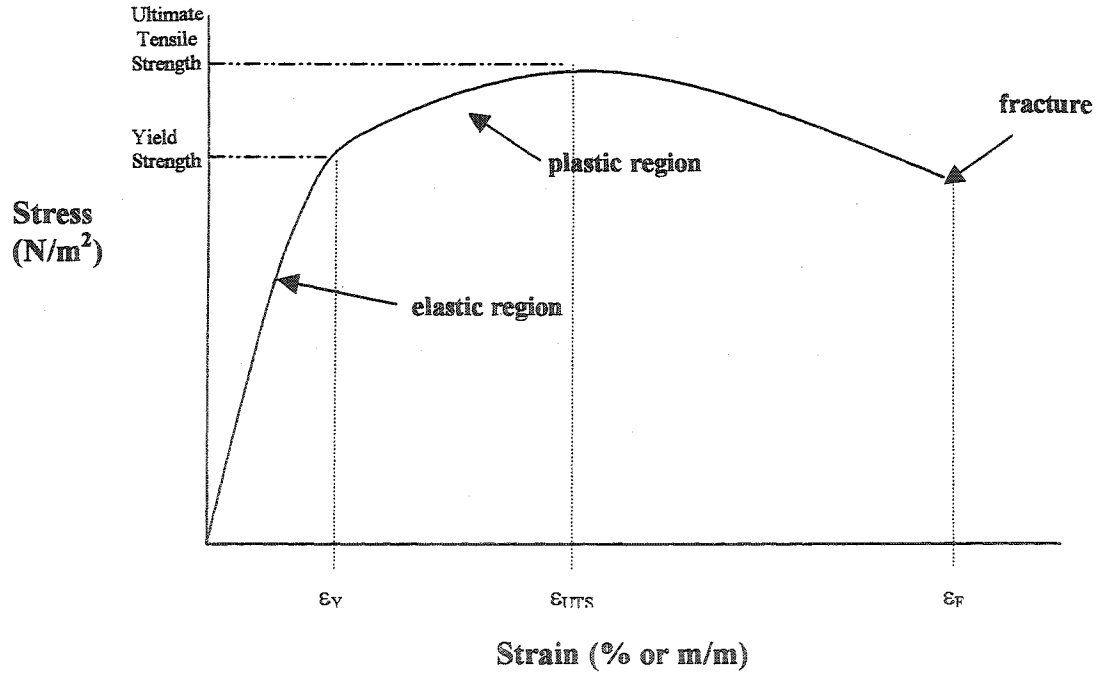

Figure 9. Representation of a stress-strain diagram for a metallic material, obtained from displacement versus load data.

For this study, a value of 30% plastic strain was chosen to represent the maximum strain that is typically found in the expansion of cardiovascular stents, these relatively high strains would be expected in regions of tightest curvature. Quantitative strain values such as these are generally determined through theoretical modeling techniques such as Finite Element Analysis (FEA), for example. An intermediate strain-value of 15% was also selected for analysis. For 316L, the strain corresponding to its ultimate tensile strength (as represented by point ε_{UTS} on Figure 9) was experimentally measured at approximately 46% for the test specimens used here, and this value served as an upper bound to which it can be strained before localized plastic deformation begins. The plastic strain in the various individual struts themselves, which allows a stainless steel stent to expand, can range from 0% to 30% within a given stent design [10].

In order to identify the effects that each surface treatment and plastic deformation has on the 316L surface the test matrix, shown in Table 4, was constructed. Treatments used in the typical processing procedures for stainless steel stents are included in the test

Table 4. Experimental Test Matrix for Critical Surface Tension (γ_{crit}) Measurements.

Elongation	Surface Treatments			
	As – received (NT)	Passivated (PA)	Electropolished (EP)	Electropolished & Passivated (EPP)
0%	X	X	X	X
15%	X	X	X	X
30%	X	X	X	X

matrix. Not included in the matrix are post-processing sterilization steps, such as Ethylene-Oxide (EtO) sterilization. The rationale for not including these sterilization steps is that, at this point in the process, the stent has already been mounted on the balloon and delivery system. Since the balloon and delivery system consist mainly of thermoplastic polymer components, such as Nylons and Polycarbonates, any post-processing sterilization procedures must limit temperature and chemical exposure to avoid degradation of the polymer components. Consequently, sterilization temperatures do not typically exceed 60°C. At these temperatures, which are approximately 0.04 times the melting point of stainless steels, there are not expected to be any physical or structural changes to the stent implant itself.

A flow-chart of the experimental testing procedure is presented in Figure 10. As seen in Figure 10, following surface treatment and plastic straining, contact angles formed by a series of liquids were measured on each surface. These data, when plotted in a Zisman format ($\cos \theta_c$ vs γ_L), enabled determination of the critical surface tension for this surface. The results of this analysis are presented in chapter 5.

4.2 Test Materials

Test specimen geometry was dictated by the requirements of both contact angle analysis and tensile testing. The use of a contact angle approach requires a flat test

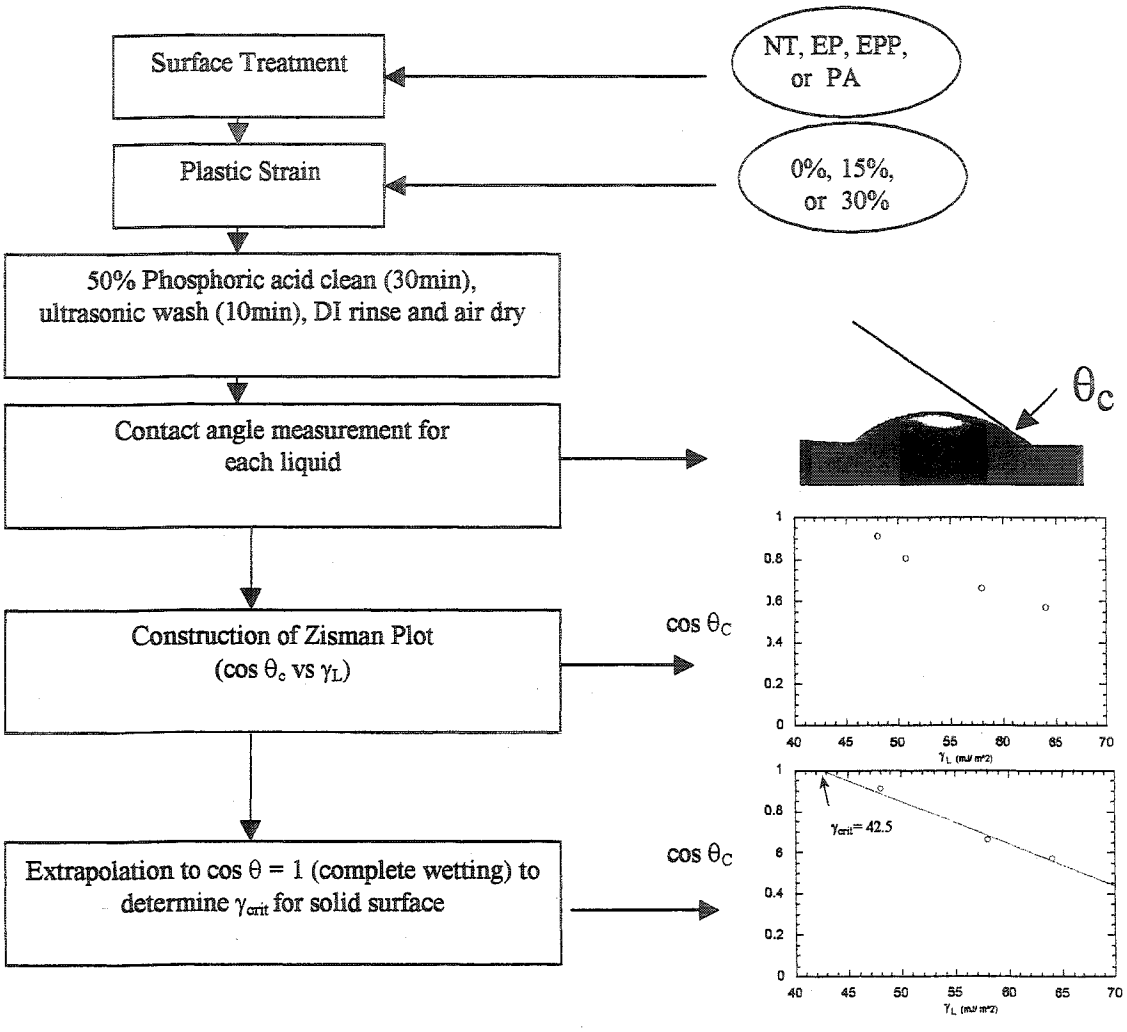

Figure 10. The experimental procedure that was used to determine critical surface tension for each surface.

surface, while tensile elongation requires a dog-bone shape of specific dimensions [39]. Therefore the test specimens were chosen to have the dimensions shown in Figure 11. The 316L test specimens were obtained stamped from fully annealed, flat, sheet stock, prepared by Laboratory Devices Co., Auburn, California. The composition of the bulk

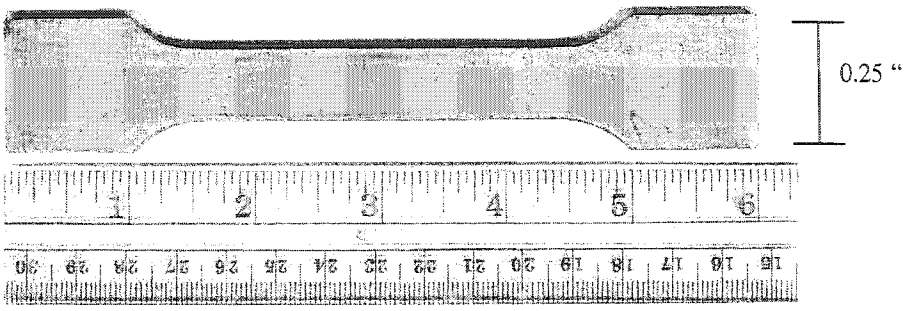

Figure 11. Photograph of as-received 316L stainless steel test specimens

316 L was verified through heat analysis to conform within the specified range for use of this material in the human body [40]. The results of the heat analysis are shown in Table 5. All specimens were from the same material lot and were supplied with a 2B surface finish, which is a general-purpose finish that is more easily polished than other standard finishes.

Table 5. Chemical Composition of the 316L Test Specimens.

C	Mn	P	S	Si	Cr	Ni	Mo	N
.024	1.76	.024	.001	.45	16.21	10.16	2.11	.04

The mechanical properties of the 316L specimens were tested to verify that they met the minimum standard requirements for in-vivo application, as specified in ASTM F745-95. A comparison of the measured results is presented in Table 6. Of particular importance for successful stent implantation, as well as minimization of stent collapse and implant-migration after expansion, is that the stent material has relatively high yield

strength. The yield strength is known to be significantly dependent on the annealing process; therefore, this parameter was verified experimentally to confirm the minimum specification for use in-vivo.

Table 6. Comparison of the Mechanical Properties of the 316L Specimens.

Source	Yield Strength (PSI)	Ultimate Tensile Strength (PSI)	Maximum Elongation (%)	Hardness (RHB)
316L Test Specimens	46,100	87,000	56	81
Minimum Specification (per ASTM F-745)	30,000	70,000	30	No requirement

4.3 Experimental Equipment

The determination of the critical surface tension, for a solid, is based upon a graphical analysis of the contact angles of a series of liquids on that surface. This necessitates measurement of accurate contact angles. Typical methods for measuring contact angles include the use of goniometers, which are microscopes fitted with special eyepieces that can measure contact angles directly. Unfortunately, there is typically no way to record and examine the data once the experiment is over, because of the lack of capability in obtaining a record of the data. Instead, the apparatus, shown in Figure 12, was assembled to measure, and record, the contact angles. This apparatus is able to image liquid droplets, and record this data onto a computer for later analysis.

was assembled to measure, and record, the contact angles. This apparatus is able to image liquid droplets, and record this data onto a computer for later analysis.

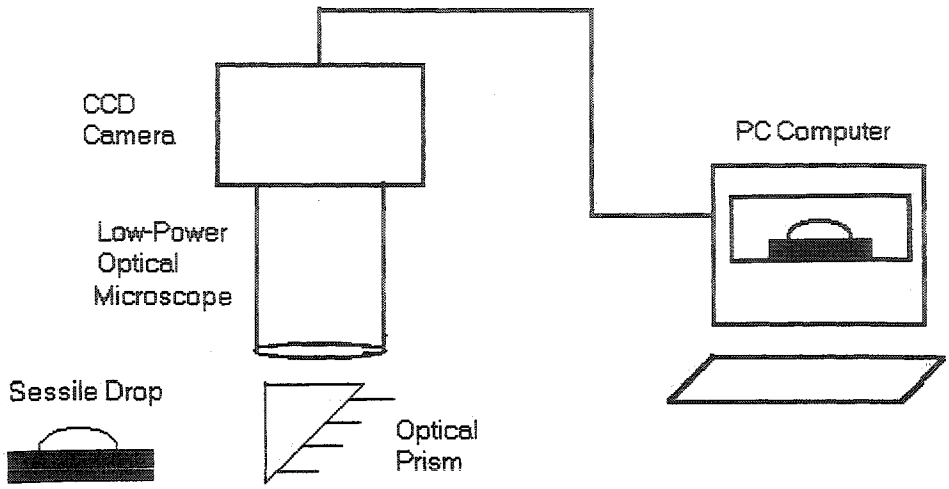

Figure 12. Contact-Angle Measuring Apparatus

Of equal importance to the contact angle analysis is the use of a variety of pure test liquids, whose surface tension has been fully characterized. The liquid surface tension must span a wide range of values, in order for a best-fit line to be accurately drawn. The liquids used in this investigation are listed in Table 7, along with their corresponding surface tension values that were subsequently used for the Zisman plots.

Although the determination of γ_{crit}, using the Zisman approach is precisely defined only for a series of homologous liquids (e.g., the n-alkane or Diether family of liquids), the use of a variety of liquids serves to minimize any biases introduced by a

result, the liquids used for this investigation encompass a variety of functional groups and have been routinely used in previous studies to in determination of critical surface tension [28, 29].

Table 7. Surface Tension Properties of the Liquids in this Study.

Liquid	$\gamma_{dispersive}$ (mJ/m^2)	γ_{polar} (mJ/m^2)	γ_{total}, mJ/m^2 ($=\gamma_d + \gamma_p$)	Source	Purity
n-decane	23.8	0	23.8	Sigma	> 99.0%
cis-decalin	32.2	0	32.2	Sigma	> 99.0%
Ethylene Glycol	29.0	19.0	48.0	Aldrich	> 99.5%
Diiodomethane	50.8	0	50.8	Sigma	> 99.0%
Formamide	39.0	19.0	58.0	Sigma	> 99.5%
Glycerol	34.0	30.0	64.0	Aldrich	> 99.5%
Water	21.8	51.0	72.8	Milli-Q (Millipore)	Resistivity ≥18.2 MΩ

4.4 Experimental Procedures

The following sections describe the procedures used to prepare each surface for contact angle and roughness measurements.

4.4.1 Surface Treatments

A summary of the four surface treatments used in this study is shown in Table 8. All surface treatments in this study were performed prior to tensile elongation, and before

measurement of contact angles. The as-received surfaces were tested with no pre-treatment performed. The electropolished (EP) surfaces consisted of as-received 316L subjected to a commercial electrolishing treatment (Pull-Bright Inc.). The passivated (PA) surfaces consisted of immersion of the as-received test specimens in a 30% nitric acid/ 70% water solution for 30 minutes at room conditions, in accordance with ASTM F86-91. The passivation solution was slowly stirred throughout using a stir-rod and stir-plate, followed by an ultrasonic wash in DI water for 10 minutes. The electropolished and passivated (EPP) surfaces resulted from a combination of the passivation treatment following the electropolish.

Table 8. Summary of Surface Treatments Tested.

Surface	Description of Surface Treatment
NT	No treatment. Specimens tested in as-received (2B finish) condition.
EP	Electropolished only. Specimens exposed to commercial electropolishing process.
PA	Passivated only, using standard nitric acid process [38].
EPP	Electropolished and passivated. Specimens passivated in nitric acid following electropolishing.

4.4.2 Tensile Elongation

Those specimens that were tested in a strained state were subjected to tensile elongation in an Instron tensile tester (model 4201). Several 316L specimens were first tested to determine the tensile properties of the test specimens, in particular, the total elastic strain; the portion of strain that is recovered after unloading. For the 316L

tested to determine the tensile properties of the test specimens, in particular, the total elastic strain; the portion of strain that is recovered after unloading. For the 316L specimens the total elastic strain, corresponding to the point ε_Y on Figure 9, was measured to be 0.53%. Therefore, to plastically strain any specimen the total strain needed was the level of desired plastic strain and an additional 0.53%. Since residual plastic strain levels of 15% and 30% were desired, the test specimens were strained to levels of 15.53% and 30.53%.

4.4.3 Specimen Cleaning

Following the surface treatment and tensile elongation procedures, the 316L specimens were subjected to a cleaning step, which immediately preceded contact angle measurements. The cleaning procedure consisted of immersion of the specimens in a solution of 50% phosphoric acid/ 50% water, stirred slowly at room temperature, followed then by an ultrasonic wash for 10 minutes in DI water. The specimens were then air-dried for approximately 3-5 minutes.

4.4.4 Contact Angle Measurement

All contact angles were measured at ambient conditions immediately following the ultrasonic cleaning and air-drying step. Test liquids were introduced onto the surfaces by means of a micro-pipette (Eppendorf P20) with sterile tips. Care was taken to avoid contact of the test liquids with the test specimen edges, due to increased stress in these areas resulting from the stamping process. Drop volumes were 15 μl per liquid,

resulting in drop diameters of approximately 4-5 mm. Droplet images were captured within 10 seconds of introduction so as to avoid a gradual decrease in contact angle with time, which occurred for a few liquids on specific surfaces. The total time to test each individual surface did not exceed 15 minutes. Test specimens that were left at room conditions for considerably longer times before testing were noticed to result in a gradual increase in measured contact angles, possibly from a re-growth of the adhered hydrocarbon layer that typically deposits on 316L.

Since contact angle measurements can be dependant on localized surface features and defects it is essential that several measurements, per condition, be taken. At a minimum three measurements, per condition, were taken for this study. In most cases, additional measurements were included when variability was observed in the first three values. The greater the number of times a measurement is repeated the greater the statistical validity, or confidence, is for that value.

4.4.5 Surface Roughness Measurements

Determinations of quantitative surface roughness parameters were done through use of Atomic Force Microscopy (AFM). All AFM scan images of the various 316L surfaces were processed with identical, user-defined, parameters. These parameters are shown in Table 9.

Calculation of quantitative roughness values for all the AFM scans was accomplished via the ProScan imaging software system. The software package allowed for calculation of roughness parameters on entire, or selected areas, within the scan

Table 9. AFM Image-Processing Parameters.

Image Parameter	Setting Used
Z-Magnification	31.07
Zoom	0.92
Z-Orientation	42.30
X/Y Orientation	Variable
Z-Offset	Variable (to keep a constant z-axis scale of approximately 5-6 μm for all images)

image. A summary of the surface roughness parameters determined for this study is presented in Table 10.

4.4.6 Calibration

To ensure the validity of the measurement system, liquid probes, and contact angle determination, calibration against a control surface is typically conducted. A standard control surface often used in contact angle measurements is the PTFE (Teflon) polymer surface. Teflon is a "low surface-energy" material that has been used extensively as a control in previous studies [28, 29,31]. The relatively low γ_{crit} of this surface, approximately 18.5 to 22 mJ/m^2, means that most liquids will form a measurable contact angle on the surface of this material; therefore, more contact-angle data points can be obtained for a Teflon surface than for a "high-energy" metallic surface. The results of the calibration measurements are presented in Section 5.2.

Table 10. Surface Roughness Parameters.

Parameter	Description
R_{median}	The median height measured from the mean plane (the mean plane is determined from a first-order least-squares-fit of height data, thereby minimizing variance of image data about this plane).
R_{avg}	Mean value of the surface relative to the center plane (the center plane is flat and divides the enclosed volume of the image surface into two equal parts).
R_{RMS}	Root mean square value of the surface relative to the center plane.
R_{P-V}	The distance between the highest and lowest points within a given area.
Projected Area	The surface area of image, no consideration given to z-axis.
Surface Area	The actual surface area of the image, which includes contributions from all peaks and valleys within the scan area.

Chapter 5
Experimental Results

5.1 Critical Surface Tension Measurements

Presented in this chapter are the results and data on the wetting characteristics of 316L stainless steel surfaces, for the specified states of surface treatment and strain. The results of the calibration measurement done with Teflon are also included within this Chapter. From the contact angle data the critical surface tension (γ_{crit}) of each test surface was determined using the Zisman technique, as discussed in Chapter 2.4.1. Also presented in this chapter are 2 and 3-dimensional topographical images taken from each of the tested surfaces. Using AFM and SEM analysis the effects of the input variables on γ_{crit} of the surfaces were analyzed.

5.2 Calibration with PTFE

To ensure the validity of the contact angle measurement system, the critical surface tension of PTFE (Teflon) was first determined. Teflon is a low surface energy material that is frequently used as a standard for critical surface tension analysis [28,29,31]. The experimentally measured contact angles on the Teflon surface are given in Table 11.

Using the data from Table 11 the resulting Zisman plot, shown in Figure 13, yields a γ_{crit} of 22.2 mJ/m^2, which is in agreement with the published range of 18.5-22 mJ/m^2 for a series of non-homologous liquids.

Table 11. Experimentally Measured Contact Angles on a Cleaned Teflon Surface.

Liquid	Mean Contact Angle (deg)	Standard Deviation (deg)	# Measurements (n)
n-decane	18.0	0.8	6
cis-decalin	28.3	2.6	7
Ethylene glycol	67.1	1.7	5
Diiodomethane	61.5	0.9	4
Formamide	79.9	2.2	5
Glycerol	81.4	3.7	6
Water	87.3	2.3	7

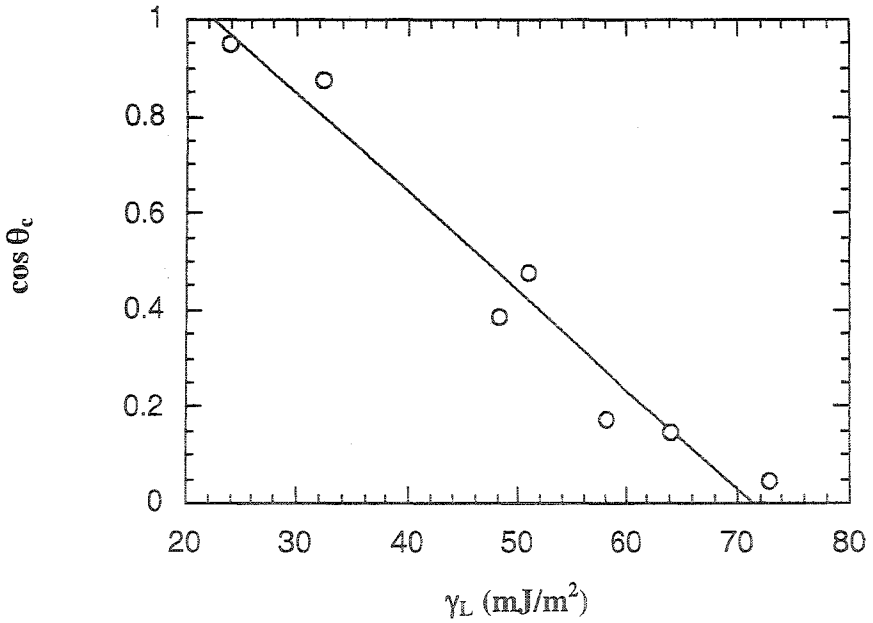

Figure 13. Zisman plot for PTFE (Teflon), based on data from Table 11.

However, the measured value of 22.5 mJ/m^2 does not take into account any effects due to the surface roughness of the Teflon. In fact, a true comparison to previously published values cannot be made without first knowing the surface roughness, texture, etc., of the surfaces in the studies. As mentioned previously, quantitative surface roughness analysis is not typically provided in these prior studies.

To quantify the surface roughness of the test specimen used in this study AFM imaging of the Teflon surface was conducted; this result is presented in Figure 14.

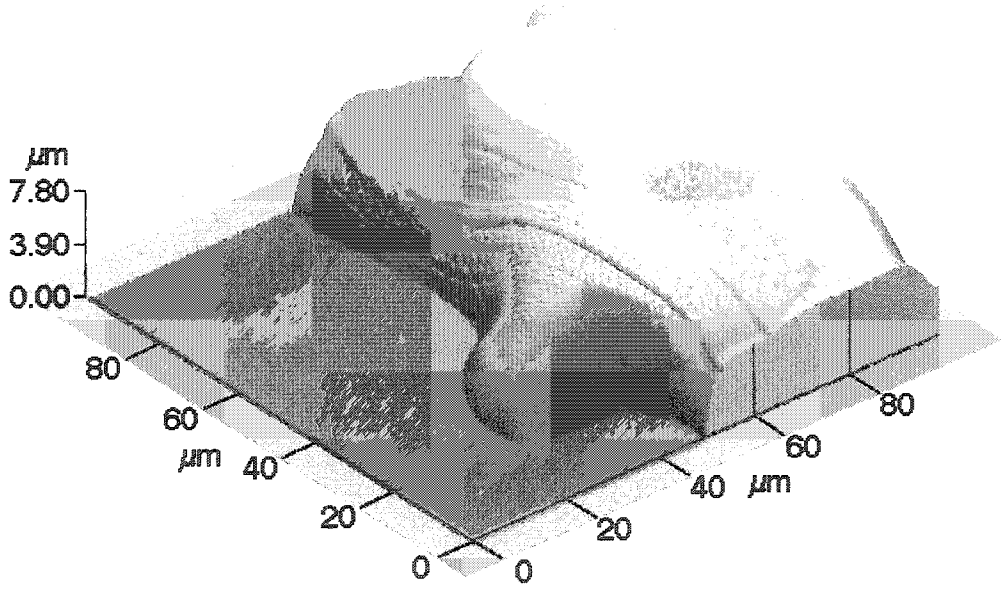

Figure 14. AFM image of Teflon surface, showing high degree of texture and relatively large surface features.

The image taken of the Teflon surface shows textured "ridges" that exceed 8 μm in height. These measurements are consistent with visual inspection of the surface, which indicates a highly textured surface with ridges that are equally spaced apart. The calculated roughness parameters for 3 scans, at different locations on the surface, are given in Table 12.

Table 12. Roughness Parameters for Teflon Surface.

Scan #	R_{median} (μm)	R_{avg} (μm)	R_{rms} (μm)	R_{p-v} (μm)	Projected Area (μm^2)	Surface Area (μm^2)	ΔS.A. (%)	Wenzel's r-value (=SA/PA)
1	4.95	3.11	3.35	> 8.0	9801	12540	21.8	1.28
2	3.90	3.28	3.47	> 8.0	9725	12480	22.1	1.28
3	3.92	3.37	3.54	> 8.0	9763	10150	3.8	1.04
Mean	4.26	3.25	3.45	> 8.0	9763	11723	15.9	1.20

The results of the AFM analysis show a significant difference in the surface area between Sample 3 and Samples 1 and 2. One reason for this is the highly textured nature of the Teflon surface, in which the observed surface ridges account for virtually all of the calculated surface roughness. Evidently, the calculated surface area difference is highly dependent on the presence of large surface features within the scanned area. The portion of the Teflon surface in Figure 14 exhibits one such example of the presence of a large surface feature. In this case, the calculated difference in surface area for this scan is

expected to be relatively small since the large surface feature dominates the scan area. The remaining portion of the scan, or plateau, is not figured prominently into the "actual" three-dimensional area calculation. The presence of localized areas of significant surface roughness helps to explain the differences in the calculated surface area differences among the scans, and likely the differences observed in the literature for this parameter.

Also calculated and included in Table 12 is Wenzel's r-value for each scan; this parameter was calculated as the ratio of the actual surface area to the projected area. The effect of the roughness factor on the Zisman best-fit line is shown in Figure 15. Roughness factors, corresponding to the minimum, maximum, and average values, measured for the Teflon surfaces were used to determine a roughness-corrected critical surface tension. A roughness factor of 1 represents the case in which no correction for roughness is considered, or, in which the observed critical surface tension is identical to the true value. The γ_{crit} determined from the roughness-corrected best-fit lines are summarized in Table 13.

The Wenzel equation, shown in Equation 6, predicts a decrease in contact angle (and an increase in γ_{crit}) with increased surface roughness, which can be seen from Figure 15 and Table 13. As an example, if the maximum value of roughness is considered (r = 1.28) the Wenzel equation predicts that the "true" value of γ_{crit} for the surface is 8.5 mJ/m2; however, the "actual" value is observed to be 22.2 mJ/m2. The difference, or increase, from the "true" γ_{crit} value is 13.7 mJ/m2, as shown in Figure 16.

Since surface roughness can directly affect the observed γ_{crit} of a surface, methods to alter a surface can be successful in achieving a desired output. For applications where

complete wetting is desired, such as adhesion of a liquid to a surface, it is desired that γ_{crit} for the solid be maximized to values in excess of the adherent liquid. In this regard, methods such as plasma treatment can be useful in raising the surface roughness, and therefore γ_{crit}.

As in the case of stent implants, previous biological studies [22,23,33] indicate that for minimization of thrombosis the opposite case is true. For these implants, a reduction in roughness and γ_{crit} is preferable. A more detailed treatment of surface roughness, for the surface conditions evaluated in this study, is contained within section 5.4.

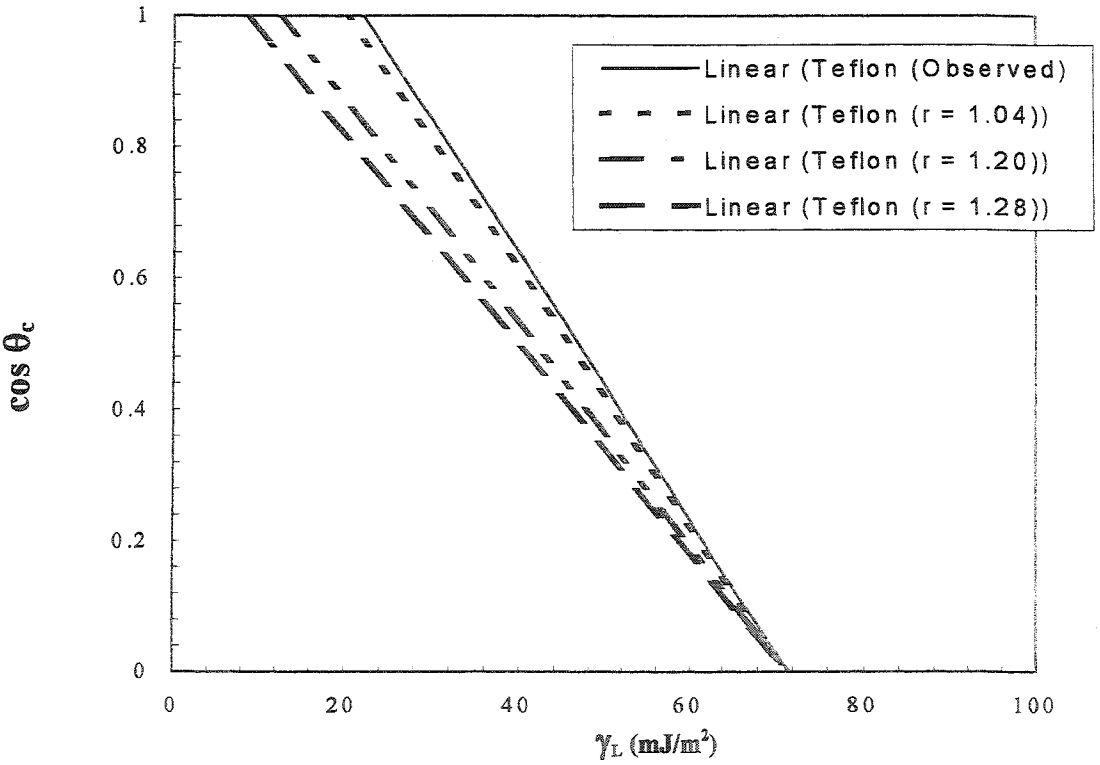

Figure 15. Comparison of the effect of the Wenzel roughness factor on the Zisman best-fit lines, for PTFE (Teflon).

Table 13. γ_{crit} Values Corrected for Roughness.

Roughness Factor, r	True Critical Surface Tension (mJ/m2)
1.04	20.3
1.20	12.4
1.28	8.5

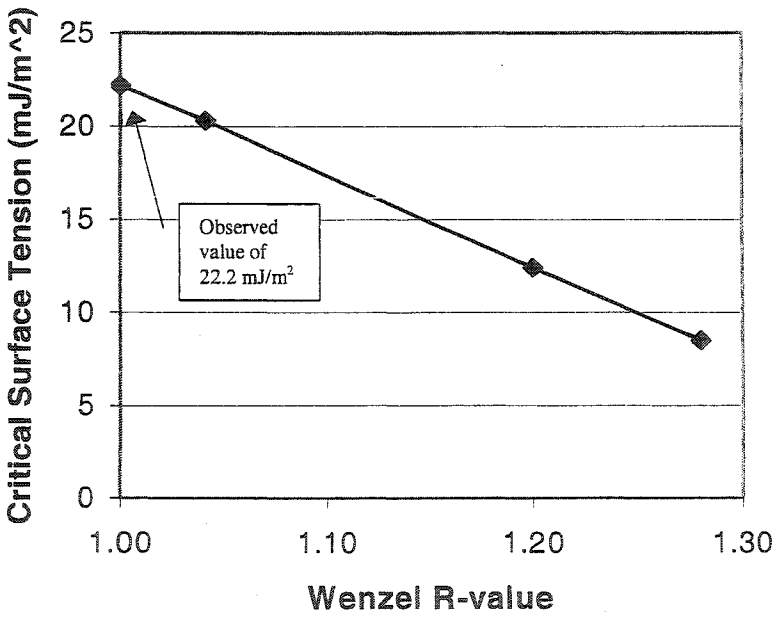

Figure 16. "True" Critical Surface Tension of Teflon, corrected for Surface Roughness

The results of Table 13 show that greater the amount of surface roughness, in the form of surface area difference, the lower the predicted γ_{crit} becomes. Published values of

γ_{crit} for Teflon, in the range of 18.5 to 22 mJ/m^2 likely illustrate the differences in the roughness among the various surfaces studied. Since surface roughness was not well characterized in previous studies, it is not possible to show an exact correlation to the results from this study.

Additional work to further alter the critical surface tension by modifying the surface roughness was not within the scope of this study. However, it can be seen from Figure 15 that changes to the observed γ_{crit} may be obtained through surface modification techniques.

5.3 Contact Angle Data on 316L Stainless Steel Surfaces

The results of contact angle measurements on all the 316L surfaces are presented in Table 14. In addition to mean values for each liquid probe, the standard deviation and total number of measurements per surface are presented for each condition. A minimum of ten (10) measurements, per condition, was targeted. In those cases where less than 10 measurements were taken either difficulty with measurements and/or limited specimens was the cause.

The data from Table 14 are presented graphically in the following four plots (Figure 17 to Figure 20) using the Zisman format. The cosine of the mean wetting angle (θ_c)is plotted as a function of the total liquid surface tension (γ_L). In each plot, the results for the three surface strain states of 0%, 15%, and 30% are also presented. Consistent with previous studies, only non-zero contact angles were plotted.

Table 14. Measured Contact Angles (θ_c) on 316L Surfaces. Values in Degrees.

Surface Treatment	Plastic strain (%)	Liquid Probes						
		Decane	Cis-decalin	Ethylene glycol	Diiodo-methane	Formamide	Glycerol	Water
NT	0	0	0	28.2 ± 7.3 (8)	37.2 ± 3.0 (8)	51.7 ± 3.1 (10)	59.4 ± 3.1 (10)	68.0 ± 5.7 (10)
	15	0	0	25.1 ± 6.0 (10)	30.0 ± 2.8 (19)	49.4 ± 3.8 (8)	60.0 ± 4.1 (10)	68.1 ± 5.3 (8)
	30	0	0	33.0 ± 2.7 (15)	32.5 ± 2.3 (15)	50.7 ± 2.9 (10)	61.9 ± 2.0 (9)	60.1 ± 7.3 (7)
PA	0	0	4.0 ± 1.1 (3)	41.1 ± 1.3 (10)	25.7 ± 2.4 (10)	46.1 ± 4.2 (10)	56.7 ± 1.7 (10)	60.8 ± 2.8 (10)
	15	0	0	40.8 ± 1.9 (6)	20.9 ± 1.9 (4)	45.2 ± 2.0 (6)	62.0 ± 1.1 (4)	69.5 ± 2.6 (6)
	30	0	0	38.2 ± 2.7 (14)	24.1 ± 1.9 (12)	43.0 ± 2.5 (14)	59.0 ± 2.9 (12)	65.4 ± 3.4 (11)
EP	0	0	0	10.7 ± 2.7 (12)	29.1 ± 2.9 (12)	22.7 ± 3.7 (6)	27.5 ± 1.8 (13)	29.5 ± 5.5 (10)
	15	0	0	19.3 ± 3.7 (15)	28.6 ± 3.0 (12)	22.5 ± 2.8 (7)	29.6 ± 4.4 (10)	18.6 ± 2.3 (7)
	30	0	0	17.5 ± 2.1 (13)	27.9 ± 2.0 (11)	19.3 ± 4.7 (11)	30.7 ± 1.4 (11)	29.6 ± 3.1 (8)
EPP	0	0	7.0 ± 1.3 (10)	23.8 ± 2.4 (10)	38.6 ± 3.0 (10)	27.8 ± 4.5 (7)	40.9 ± 3.9 (8)	37.8 ± 3.2 (6)
	15	0	3.5 ± 0.5 (3)	30.2 ± 3.6 (10)	33.5 ± 3.0 (10)	28.1 ± 3.6 (7)	39.4 ± 3.5 (7)	41.5 ± 4.2 (6)
	30	0	3.7 ± 1.7 (3)	26.6 ± 3.8 (8)	25.2 ± 3.2 (10)	25.4 ± 1.9 (15)	37.2 ± 3.8 (10)	37.4 ± 2.2 (8)

* Measurements are mean values with ± 1σ. The number of individual data points that were averaged are given in parenthesis.

5.3.1 Results of Contact Angle Measurements on Untreated 316L

The results for the as-received untreated surfaces are plotted in Figure 17. Consistent with the rough visual appearance of the untreated surfaces, which were supplied in a 2B surface finish, the data resulted in relatively large γ_{crit} values, > 40 mJ/m^2, for all extents of surface strain. With respect to Figure 17, the large γ_{crit} values for the NT surface demonstrate a material better suited for bio-adhesion (maximum reactivity) rather than blood compatibility. Surface strain itself did not appear to have a significant effect on the wetting behavior. A more detailed statistical treatment of the data is given in section 5.2.4.

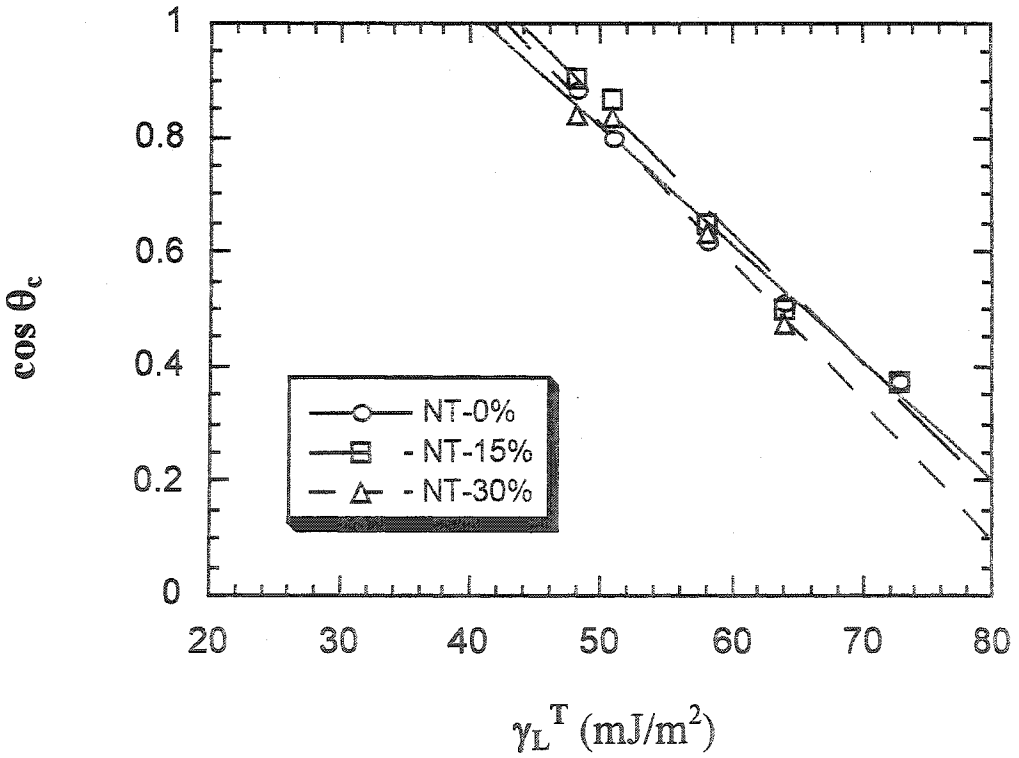

Figure 17. Zisman plots for the non-treated (NT) surfaces, with the indicated amount of surface strain.

5.3.2 Results of Contact Angle Measurements on Passivated 316L

The as-received 316L test specimens, after exposure to a passivation process in accordance with ASTM F 86-91, yielded the results shown in Figure 18. Although a visual inspection of the surfaces immediately following passivation did not reveal a noticeable difference from that of the untreated surfaces, the wetting behavior of the liquid probes, in response to the surface, was nonetheless different. In particular, cis-decalin ($\gamma_L = 32.2$ mJ/m^2), which was observed to completely wet the untreated surfaces, was found to have a measurable (non-zero) contact angle following the passivation process. The Zisman plot for the PA surfaces, in comparison to the NT surfaces, demonstrated a slight reduction in the slope of the best-fit line. The reduction of the

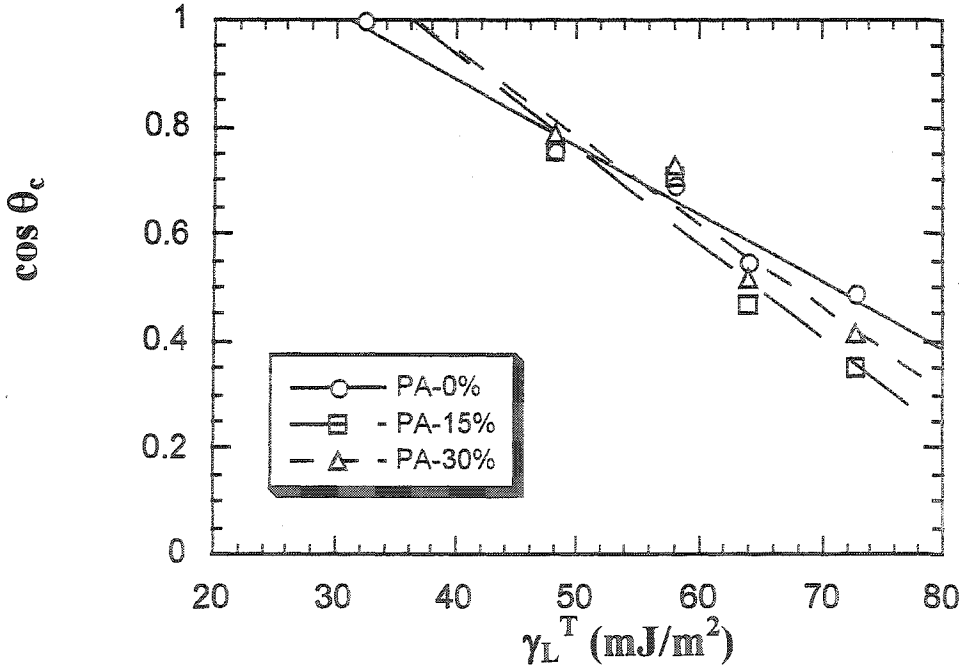

Figure 18. Zisman plots for the passivated only (PA) surfaces, with the indicated amount of surface strain

slope results in lower γ_{crit} values, between 30 to 40 mJ/m^2, compared to the NT group. From a biocompatibility perspective, the shift in γ_{crit} indicates a surface that would be expected to provide a more favorable response in a blood environment. Similar to the NT group, surface straining did not have a significant effect on the results.

5.3.3 Results of Contact Angle Measurements on Electro-polished 316L

In Figure 19 is shown the results of the electropolished surface. In contrast to the NT and PA surfaces, the EP group was visibly smooth and had a mirror-like appearance.

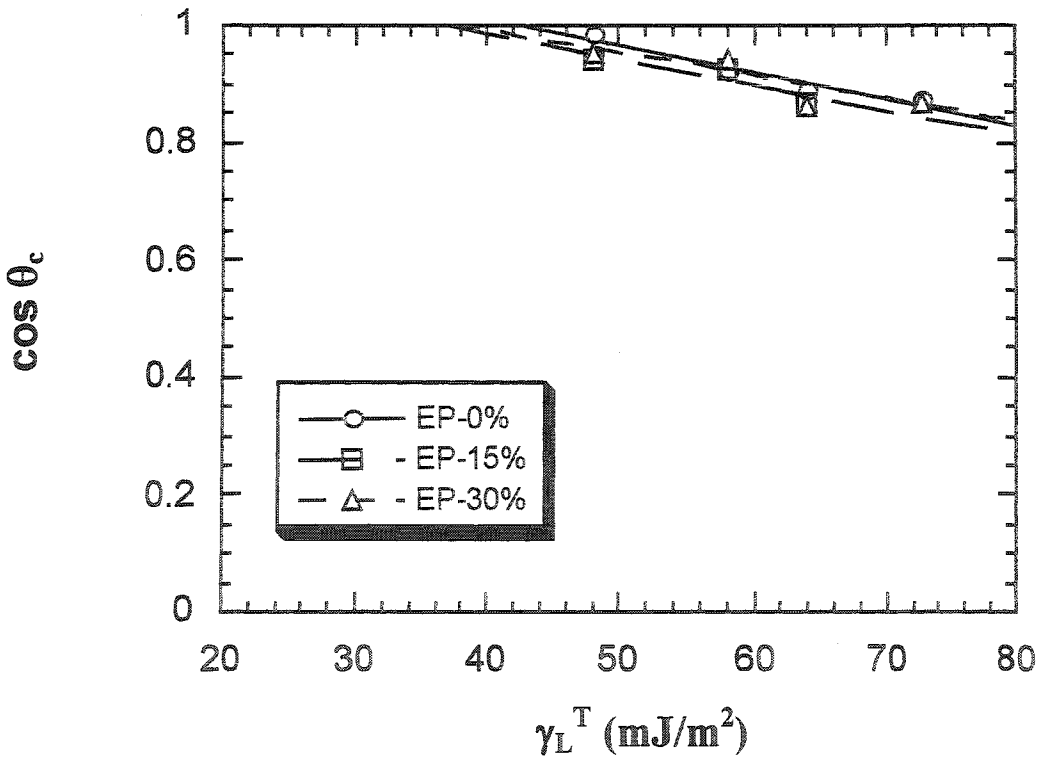

Figure 19. Zisman plots for the electro polished only (EP) surfaces, with the indicated amount of surface strain

5.3.4 Results of Contact Angle Measurements on Electro-polished and Passivated 316L

In Figure 20 is shown the results of the electropolished and passivated (EPP) surface. Similar to the EP surface, the EPP surface was also visibly smooth and mirror-like, although not as brilliant as the EP surface finish. The finish on both the EP and EPP were visibly different than the NT and PA surface.

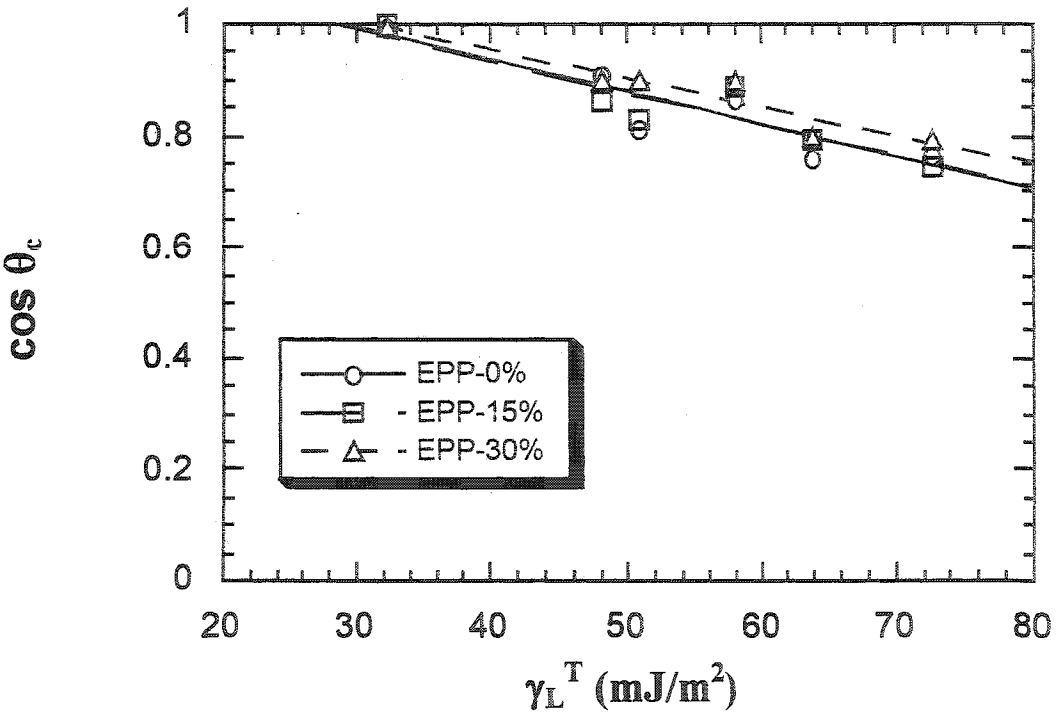

Figure 20. Zisman plots for the electro polished and passivated (EPP) surfaces, with the indicated amount of surface strain

The difference in appearance also resulted in significant differences in the wetting of the liquid probes on these surfaces. In general, all liquids, with the exception of diidomethane, were found to exhibit lower contact angles on the EP and EPP surfaces.

Typically, a trend toward lower contact angles would indicate a surface with increased critical surface tension, this is because as the contact angles decrease the cos θ_c values increase and this effectively shifts the best-fit line upwards. The assumption here is that the slopes of the best-fit lines are constant for all materials. In general, values for this parameter has been experimentally found to lie within the range of 0.02 to 0.04, similar to the values of the NT and PA surfaces here. However, the electro polishing process evidently causes a significant decrease in the slope of the best-fit line, which results in relatively lower γ_{crit} values for both electro polished groups (EP and EPP). In particular, the EPP group was found to have the lowest γ_{crit} of all the surface conditions tested in this study. With the exception of the unstrained PA surface, the EPP surfaces were the only group on which cis-decalin formed a non-zero contact angle, indicating a γ_{crit} less than 32.2 mJ/m^2 for these surfaces. A summary of the Zisman plot findings is presented in section 5.2.5.

5.3.5 Statistical Analysis of Wetting Data

In order to determine statistically significant differences in the measured contact angles, resulting from the effects of surface treatment, a Two-Sample T-Test was conducted for comparing two means. The only requirements for this analysis are that both populations be independent and normally distributed [43]. The calculated t-value is determined according to Equation 7:

$$t = x_1 - x_2 \,/\, (s_1^2/ n_1 + s_2^2/ n_2)^{0.5} \qquad \text{Equation 7}$$

where x_1 and x_2 are the means of samples 1 and 2, s_1 and s_2 are the standard deviations of the two samples, and n_1 and n_2 are the sizes of the two samples. The number of degrees of freedom for each calculation is the smaller of n_1-1 and n_2-1.

A sample calculation, comparing the contact angle of ethylene glycol on the NT-0% surface and PA-0% surface is shown below. The t-value was calculated from Equation 11 to be

$$t = 41.1 - 28.2 / (1.3^2/10 + 7.3^2/8)^{0.5} \qquad \text{Equation 8}$$
$$= 4.936$$

The degrees of freedom are 8-1 = 7. The critical t-value is determined from a table of values [43], and in this case, the two-sided critical value for a 95% confidence level with 7 degrees of freedom is 2.365. Since the actual t-value of 4.936 exceeds the critical value of 2.365, the wetting angles of ethylene glycol for the two surfaces were found to be statistically different, at the 95% confidence level. Repeating this calculation, for the indicated liquids, yields the results shown in Table 15.

The results of the statistical analysis demonstrate that, relative to the initial state of the surface, each subsequent treatment to the surface resulted in statistically different contact angles for the same liquid. The one exception was on the EP surface, where following the passivation treatment there was no statistical change in the contact angle of the formamide liquid. Nonetheless, the results of the table show that the PA and EP treatments resulted in statistically significant differences in the contact angles, with the

Table 15. Statistical Comparison of Contact Angles Taken on the Unstrained States.

Surface Comparison: NT and PA					
Liquid	**Ethylene glycol**	**Diodomethane**	**Formamide**	**Glycerol**	**Water**
t-value	4.936	8.818	3.392	2.415	3.585
t-critical	2.365	2.365	2.262	2.262	2.262
statistically different	yes	yes	yes	yes	yes
Surface Comparison: NT and EP					
t-value	6.491	5.995	16.981	28.141	13.993
t-critical	2.365	2.365	2.447	2.262	2.447
statistically different	yes	yes	yes	yes	yes
Surface Comparison: EP and EPP					
t-value	12.042	7.508	2.316	8.983	3.381
t-critical	2.262	2.262	2.447	2.365	2.571
statistically different	yes	yes	no	yes	yes
Surface Comparison: PA and EPP					
t-value	20.043	10.618	8.480	10.676	14.574
t-critical	2.262	2.262	2.447	2.365	2.571
statistically different	yes	yes	yes	yes	yes

exception noted above. Consequently, any differences in the critical surface tension values from these contact angle data can also be expected to be statistically significant.

5.3.6 Summary of Critical Surface Tension Measurements

Following the Zisman method, as discussed in section 2.4.1, for determining critical surface tension values (γ_{crit}) from contact angle data, best-fit lines were drawn

through the data points of Figure 17 through Figure 20 and extrapolated to values of γ_L that correspond to cos θ_c =0. The results of the best-fit lines, for each surface condition, allow for the determination of γ_{crit} via Equation 5. From the linear fits, the slope (b) was also determined. The results of the best-fit process are shown in Table 16, which also includes the R-values indicating the "goodness of fit."

Table 16. Summary of Experimentally Determined Values of Critical Surface.

Surface Treatment	**Surface Strain (%)**	**γ_{crit} (mJ/m^2)**	**Slope of the best-fit line (m)**	**Goodness of Fit (R)**
NT	0	40.9	.016	0.96
	15	43.7	.022	0.99
	30	42.6	.024	0.97
PA	0	31.6	.013	0.99
	15	36.2	.017	0.95
	30	36.4	.016	0.95
EP	0	42.5	.005	0.97
	15	36.6	.004	0.92
	30	37.3	.004	0.85
EPP	0	28.8	.006	0.91
	15	28.5	.006	0.91
	30	31.2	.005	0.95

The data in Table 16 allow for determination of γ_{crit} as a function of both input variables - surface treatment and surface strain. This overall summary of the results is

presented in Figure 21; superimposed on the plot is Baier's "Hypothetical Range of Surface Biocompatibility [33]."

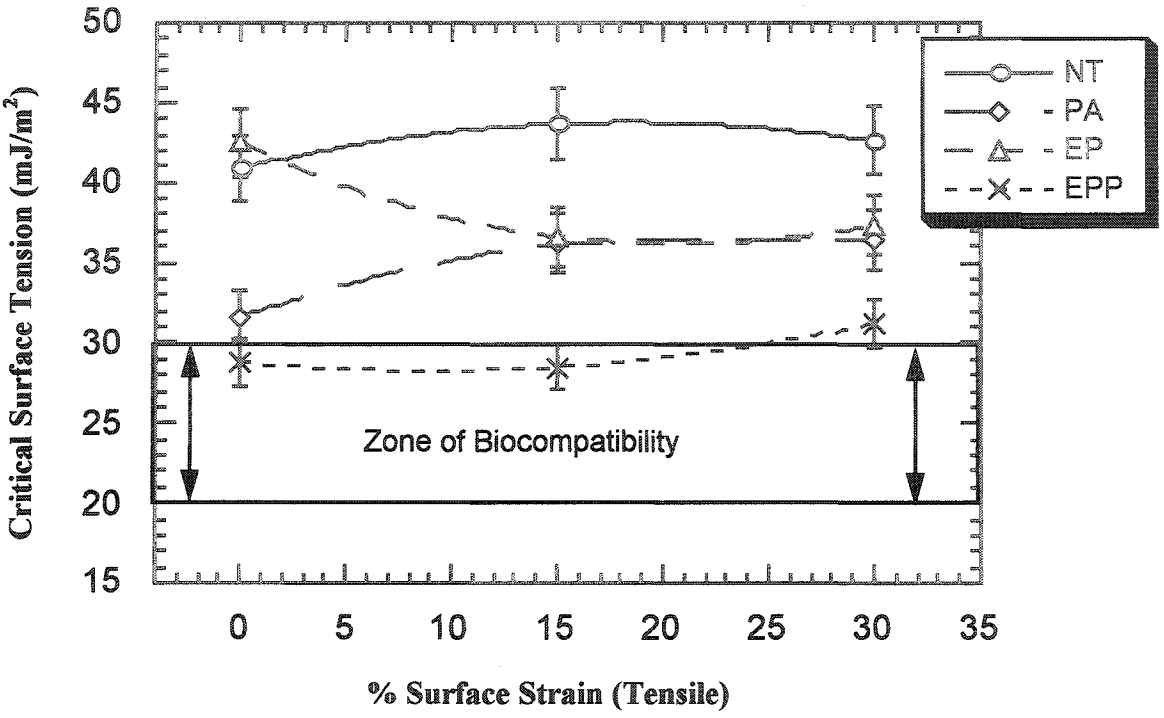

Figure 21. Critical surface tension (γ_{crit}) as a function of elongation and surface treatment

From Figure 21 it can be seen that changes in surface treatment has a far greater effect on γ_{crit} than does changes in the surface strain (tensile in this case).

In general, the order of γ_{crit} for the surfaces tested are NT > EP > PA > EPP, with EPP being the only surface treatment that yielded γ_{crit} values within the zone of biocompatibility.

The untreated (NT) surfaces exhibited the largest γ_{crit} values among the test groups, and for a blood-contacting material would be expected to be the least compatible and most thrombogenic. The electropolishing process served to improve the biocompatibility of the as-received 316L surface, by decreasing the range of γ_{crit} from values representative of metallic materials to those approaching a polymeric material (approximately 34-38 mJ/m^2).

Passivation of the surfaces, either to the as-received 316L or following electropolishing, resulted in surfaces that would be expected to perform better in a blood-contacting environment, when compared to the un-passivated state. The reason for this is because passivation of these surfaces served to decrease γ_{crit}, regardless of the condition of the surface initially. For the case of an initially untreated surface (NT), passivation resulted in a decrease of γ_{crit} by approximately 6-9 mJ/m^2. For the initially electropolished surface (EP) the reduction was approximately 6-13 mJ/m^2. In both cases a more favorable biocompatibility outcome can be expected following the passivation surface treatment. Most significantly, the resultant γ_{crit} for the EPP surface (passivation following electropolishing) was the only surface to lie within the proposed "Biocompatible" zone. This indicates that, with respect to surface tension, the combination of electropolishing followed by passivation served to render the external appearance of the surface more representative of a Teflon material, instead of a 316L stainless steel. The importance of the change to a more "Teflon-like" surface indicates that, from the perspective of the blood environment, the EPP treated surface is now more likely to follow the "low-energy" pathway of Figure 8, as opposed to the "high-energy"

pathway that eventually leads to thrombosis. The result, from a patient perspective, is that a 316L stent treated with the EPP condition is the most likely surface, among the tested groups, to result in a favorable clinical outcome, which is defined as a reduction in the occurrence of either acute or sub-acute thrombosis.

5.4 Atomic Force Microscopy Measurements on 316L-SS Surfaces

In section 5.2 a relationship between surface treatment and critical surface tension (γ_{crit}) was established. No effort was made to determine the nature of the change in the surfaces, which led to their differences in wetting behavior. In this section the surface topography of each group will be investigated to determine the effects of the input variables (surface treatment and strain) on the topography, and therefore any relationship between topography (roughness) and γ_{crit}. The analysis methods consisted of both quantitative, Atomic Force Microscopy (AFM), and qualitative, Scanning Electron Microscopy (SEM), methods.

5.4.1 AFM Topography Results for Each Surface Condition

AFM scans of each 316L surface condition, specified in the test matrix, are shown in Table 17.

5.4.2 Quantitative Measurements of Roughness Parameters

The data presented in Table 17 show that the as-received (NT) 316L surface possesses a rough, textured, appearance of uneven heights. Upon straining, the NT

surface exhibits an elongation of the grains in the x-y axis at lower degrees of strain. However, at higher degrees of strain the NT surface becomes increasingly rough and inconsistent. This is an observation that is applicable to each surface: at low degrees of strains the surfaces almost appear smoother than the unstrained states. However, at higher degrees of strain all surfaces become increasingly rough and lose any texture that was present in the unstrained states.

Table 17. AFM Topography Scans for Each Surface Condition

Surface	Surface Strain (%)		
	0	15	30
NT	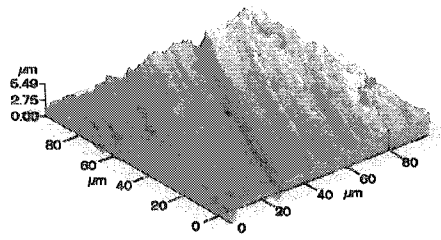	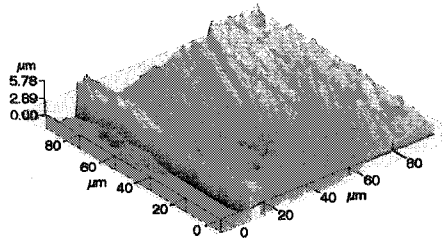	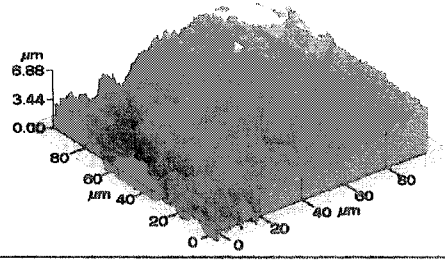
PA	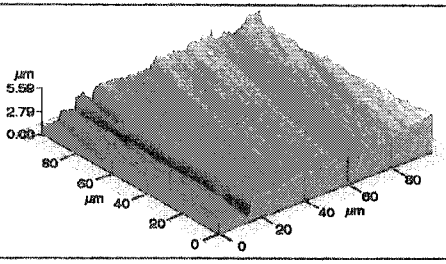	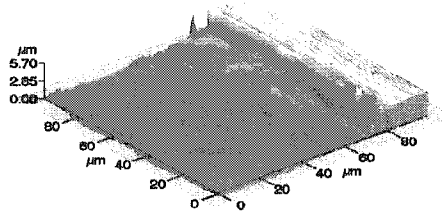	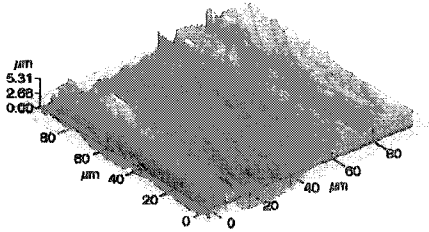
EP	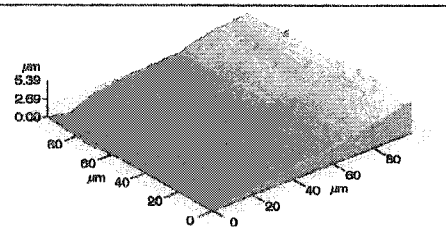	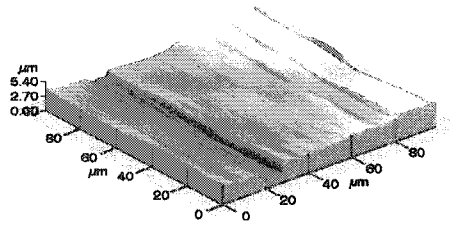	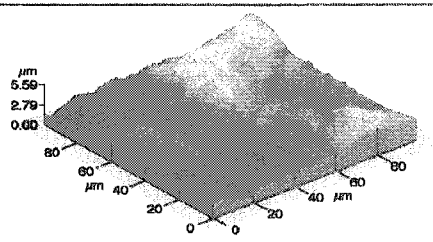
EPP	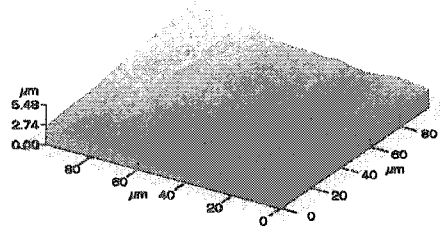	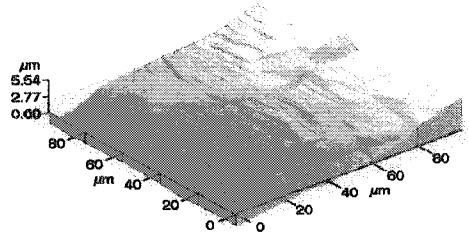	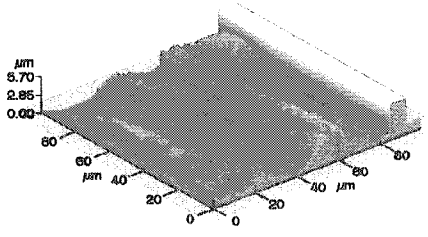

Note: The areas beyond approximately 80 microns for the PA-15% and EPP-30% specimens were not used for calculation of roughness parameters since these portions of the plots represent where the AFM tip was damaged.

From previous work it is known that roughness affects the observed critical surface tension of a solid [32,36]. To quantify the relationship between surface roughness and γ_{crit} the surface roughness parameters were calculated, and are presented in Table 18

The effect of elongation on the measured surface roughness is particularly significant in the peak to valley roughness (R_{p-v}) of the non-passivated surfaces. The EP and EPP surface not only had a lower degree of R_{p-v}, but also had values that were not affected by elongation to the degree of the NT and PA surfaces.

Table 18. Calculated Roughness Parameters for 316L Surfaces.

Surface	% Elongation	R_{median} (μm)	R_{rms} (μm)	R_{avg} (μm)	R_{p-v} (μm)	Surface Area Diff. (%)
NT	0	4.11	1.31	1.09	7.22	15.21
	15	3.13	1.88	1.64	7.92	17.15
	30	4.06	2.08	1.67	> 8.0*	25.13
PA	0	3.03	0.94	0.72	5.31	11.89
	15	1.18	0.93	0.77	5.77	9.53
	30	3.63	1.71	1.40	> 8.0*	37.21
EP	0	2.32	1.34	1.16	6.08	4.66
	15	5.49	0.70	0.50	7.56	9.83
	30	2.59	0.96	0.76	5.75	6.30
EPP	0	2.33	1.13	0.94	5.62	4.94
	15	3.33	2.0	1.73	7.45	1.73
	30	1.68	1.21	0.95	6.73	12.59

* The upper limit of measurement for peak-to-valley distance is 8 microns.

5.4.3 Summary of Surface Roughness Measurements

To evaluate the effect of surface treatments on the roughness of each surface, the average roughness from Table 18 was plotted as a function of treatment. This plot is shown in Figure 22.

The comparison of the average surface roughness in Figure 21 demonstrates a relationship between surface treatment and roughness, when exposed to the passivation process. The relationship is that as an initially untreated, or eletropolished, 316L surface is passivated the result is a decrease in the average surface roughness. This finding is consistent with the expected nature of the passivation process itself, which is to create a more consistent surface texture through growth of a uniform oxide layer. However, based on the visual comparison of untreated and electroplished specimens, the same expectation of decreased surface roughness should also be true of the electropolishing

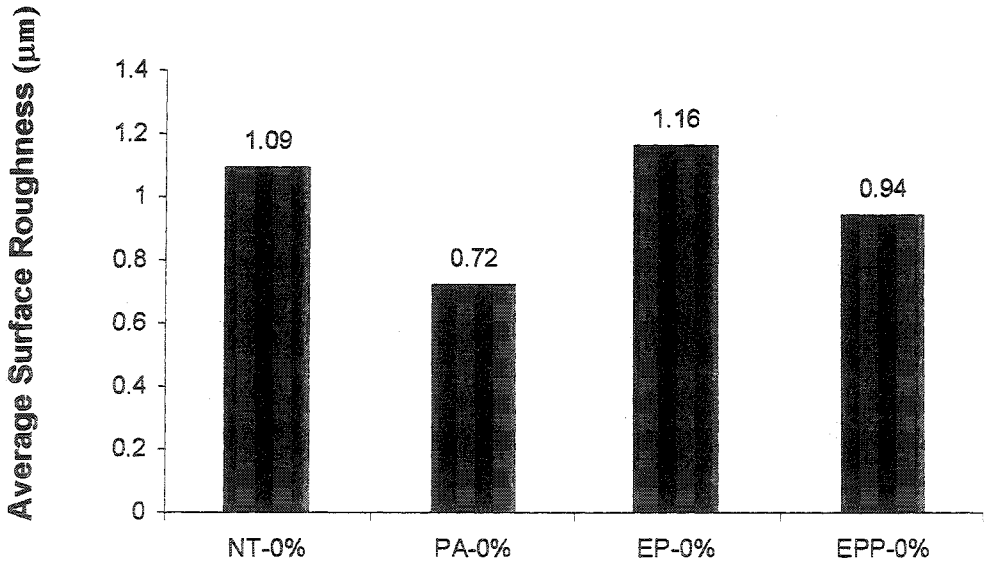

Figure 22. Average Roughness for Each Unstrained Surface Condition

treatment. Yet, the average roughness was found to increase following the EP treatment. This apparent contradiction can be explained by the "nature" of the roughness of each surface. Since the average roughness calculation is based on calculation of the surface above and below a center-plane, if a surface has roughness that is random then the net result will be a surface with apparent low roughness. However, if a surface has texture that is not necessarily random then the average roughness will appear greater. In the case of the EP surface it is known that the electropolishing process selectively removes material from surface peaks, so for the EP surface the peaks are reduced but valleys are also deepened. The result is that the EP surface is "smooth," as evidence by the lowest surface area difference among the group and by the brilliance of shine from the surface; however, the many valleys of the surface contribute to a measured "rough" surface that is evident in Figure 22. This unexpected result of the EP surface also serves to explain the behavior observed for this surface in the critical surface tension analysis (Figure 21), which was that the unstrained EP surface was measured to have a γ_{crit} larger than even the untreated 316L. This correlation between the surface roughness and critical surface tension behavior of the EP surface is consistent at all levels of strain, as evident by the plot of the average surface roughness shown in Figure 23.

Although the trend of the average roughness curve for the EP surface does follow that of the same surface in the critical surface tension plot, the values obtained for the EP surface are larger than those of the EPP surface. This finding however does not correlate with the results of Figure 21, which suggest that the EPP surface should have the lower average roughness, if in fact roughness was the only mechanism driving the differences

in critical surface tension. Examination of the non-electropolished surfaces (NT and PA) shows trends that are not only consistent with those in Figure 21, but also consistent in their relative positions to each other in both plots.

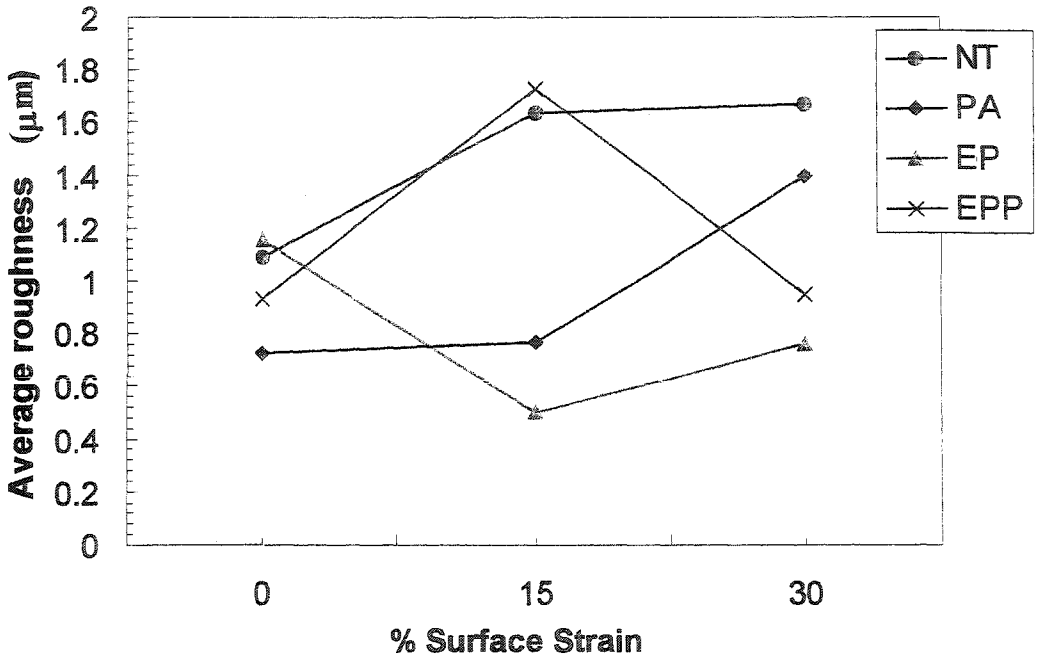

Figure 23. Average surface roughness as a function of tensile elongation and treatment.

A better correlation between roughness and γ_{crit} is evident when the Surface Area difference is plotted for each condition, as shown in Figure 24. In this case there is better correlation across all surface treatments with the γ_{crit} results, in accordance with Wenzel's definition of the roughness factor (Equation 6). Spurious data points, such as the 30%

strained PA surface, may be due to localized surface defects that may not necessarily be representative of the general surface state.

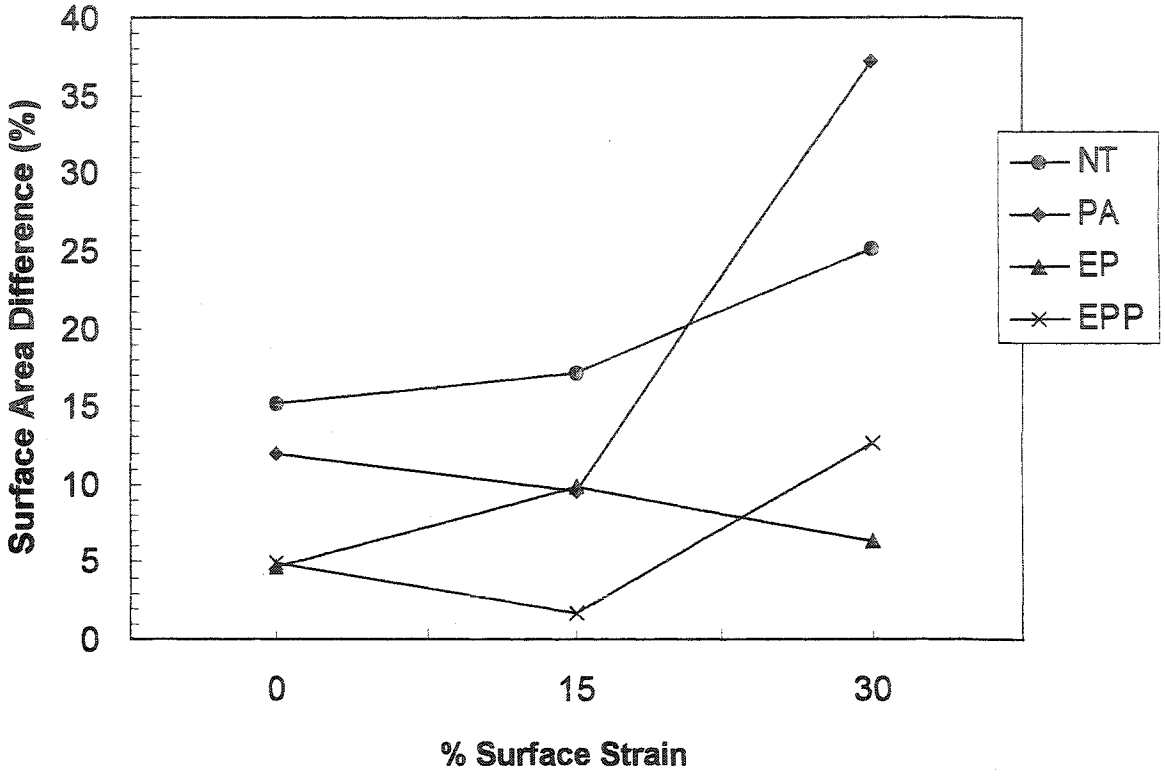

Figure 24. Surface area difference as a function of tensile elongation and treatment.

5.5 Scanning Electron Microscopy Results

Two-dimensional topographical images of each of the surface treatments are presented in Figures 25-28. Only the extreme values of surface strain (0% and 30%) were imaged, since the intermediate 15% strain condition is assumed to provide a surface image intermediate to the extreme images presented here. All SEM images shown were taken at identical angle, magnification and beam intensity.

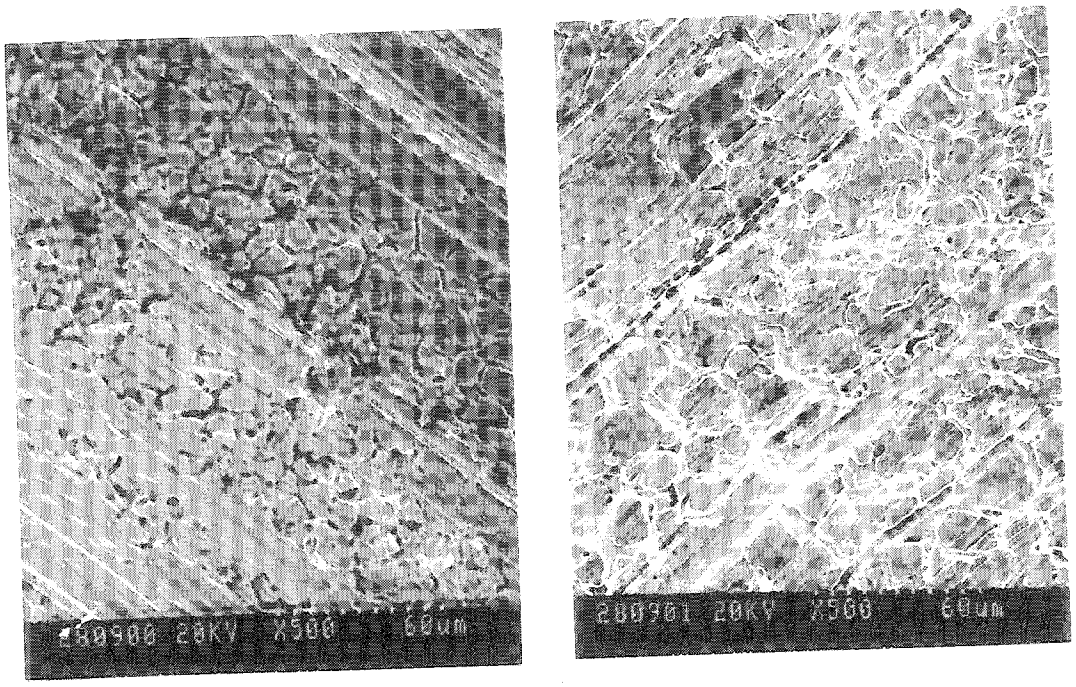

Figure 25. SEM images of a) unstrained NT surface and b) NT after straining to 30%

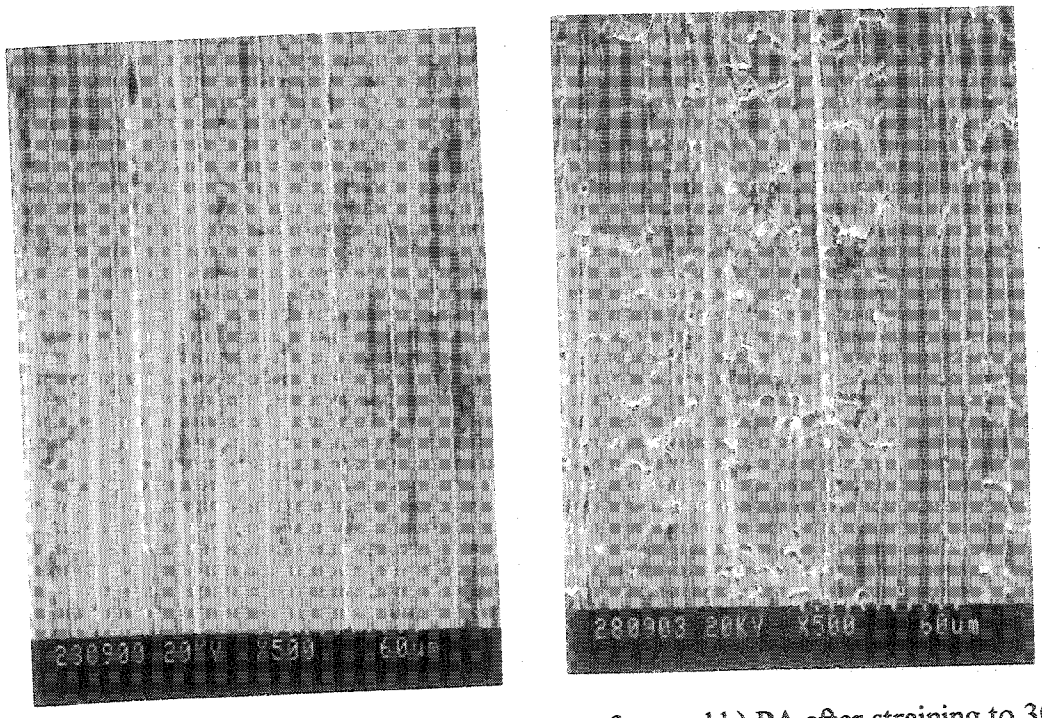

Figure 26. SEM images of a) unstrained PA surface and b) PA after straining to 30%

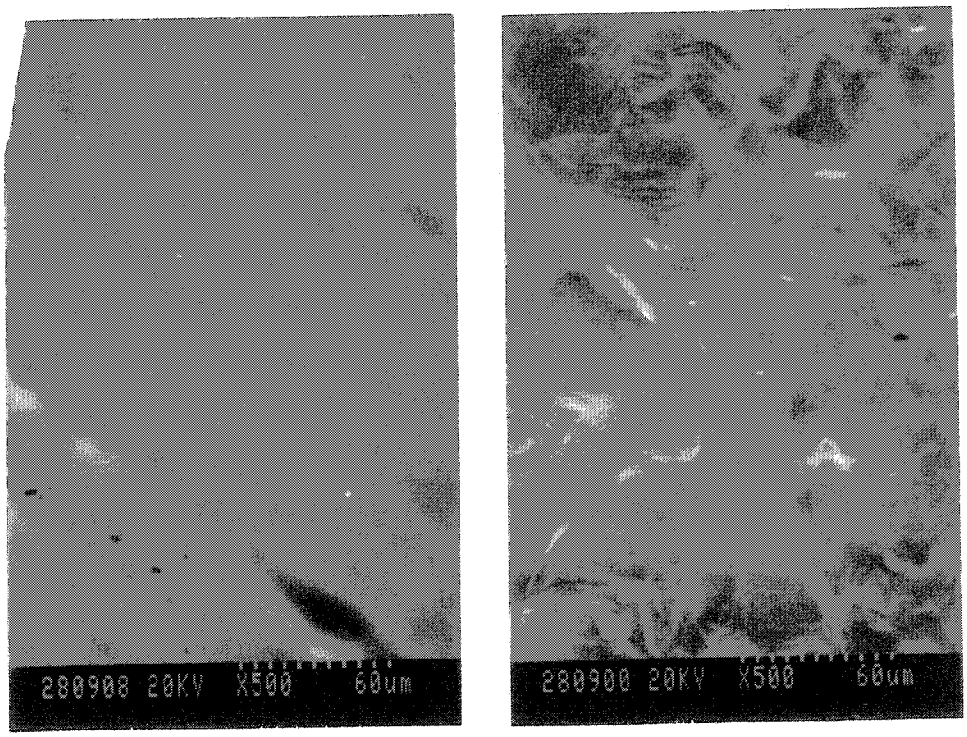

Figure 27. SEM images of a) unstrained EP surface and b) EP after straining to 30%.

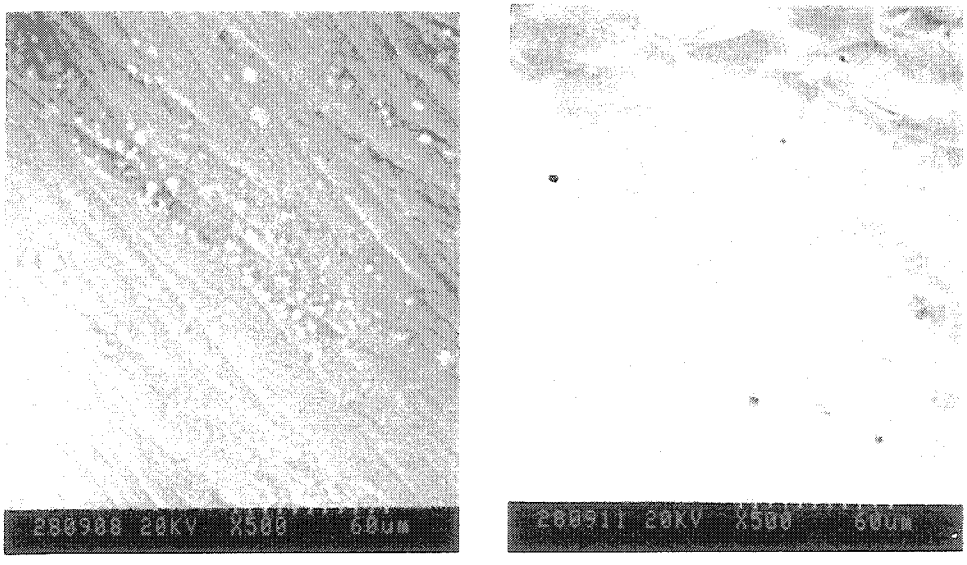

Figure 28. SEM images of a) unstrained EPP surface and b) EPP after straining to 30%.

The results of the SEM analysis provide complimentary information to the AFM data presented in section 5.4.3. The effect of the passivation treatment, in creating a more uniform oxide layer, is more pronounced in Figure 27. In the unstrained image of the PA surface are absent the rough oxide scales shown in the as-received image of Figure 25a, this is consistent with the corresponding AFM image in Table 17. The unstrained EP surface in Figure 27 shows pronounced "valleys" that are consistent with the explanation provided in Section 5.4.3, which was that the EP surface is considered a relatively rough surface when viewed in terms of average surface roughness. The absence of these valleys in the EPP image of Figure 28 also supports the hypothesis that the reduction in critical surface tension is due primarily to surface roughness effects.

Chapter 6

Discussion of Results

6.1 Introduction

The effectiveness of a stent to maintain biocompatibility, as it is gradually incorporated into the body, is dependent on the chemical and biological interactions of the implant surface and the (external) blood environment at the time of implantation. In this *in-vitro* study surface energy and surface topography of the implant material 316L stainless steel were studied to determine their role in the *in-vivo* events occurring at the time of implantation.

6.2 Effect of Surface Treatment and Tensile Strain on Critical Surface Tension

Two important liquids frequently used in critical surface tension analysis are diiodomethane and water. The importance of diiodomethane results from the fact that this liquid supports no hydrogen-bonding components, reference Table 7, and therefore its contact angle gives an estimate of the dispersive (Van der Waals) component of a given solid surface. The dispersive component of a solid's surface tension (γ_S^d) has been reported to be independent of the crystallinity of a surface, or any mechanical strains [30]. In contrast, water is predominantly composed of polar (hydrogen-bonding) components; therefore, its contact angle is more sensitive to a solid surface's polar characteristics and is expected to be more an indication of surface chemistry rather than topography.

The roles of the polar (γ_S^p) and dispersive (γ_S^d) components of a solid are relevant when examining the Zisman plots of Figure 17 through Figure 20. Even though the Zisman plots for the EP and PA surfaces yield similar γ_{crit} values, of 35-40 mJ/m^2, the large difference in slope of the best-fit lines indicate a change in the contact angles of the liquid probes on these surfaces. The difference in the wetting patterns on these surfaces gives some detail into the nature of the surface itself, as well as the function of a given external process – such as surface treatments or tensile elongation.

For the untreated (NT) 316L surfaces the wetting pattern of the liquid test series yielded the highest range of γ_{crit} values (41-44 mJ/m^2), as well the largest values for the slope of the best-fit line– comparable to that of the Teflon surface. However, unlike Teflon, which is known to exhibit good biocompatibility with blood, the as-received 316L resulted in γ_{crit} values approximately twice as large. This confirms a fact already known to be true in practice - that untreated stainless steel in contact with blood can be very thrombogenic. In fact, untreated stainless steel has been used in thrombogenic models to consistently induce thrombus formation in animals [13].

The effect of the passivating treatment served to reduce the critical surface tensions of both the untreated, and electropolished, surfaces as shown in Figure 17 through Figure 19 and Table 16. This is in contrast to the results of identical passivation treatments on TiO_2 surfaces, as shown in Table 3. The passivation treatment, when applied to the 316L surface, creates a more stable oxide layer through preferential oxidation of the chromium; in the absence of electropolishing, passivation is used to prepare the surfaces of metallic implants for *in-vivo* implantation [37]. The improvement

in the appearance of the surfaces was evident in the AFM and SEM images of the unstrained PA surfaces. In comparison to the NT specimens, the PA surfaces appear more uniform in the heights of the surface features within the scan area, as evident from a comparison of the roughness values shown in Table 18. The improvement in surface uniformity appears to result from a removal of the initially rough surface oxides by the nitric acid solution, followed by a re-growth of a more consistent oxide layer. This function of the passivation treatment is consistent with previous reports as well [41]. Since nitric acid passivation of 316L is usually performed at room temperatures, changes in the oxide thickness are not usually observed. In this study nitric acid passivation at ambient conditions resulted in a lowering of the critical surface tension. The effect of oxide layer thickness on the critical surface tension has not yet been explored.

The electropolishing treatment, which is intended to smooth out the surface following the forming process, is known to result in a chromium-enrichment at the surface of approximately 1.5 times that of iron. The increased chromium present at the surface then reacts with oxygen to result in the formation of a uniform chromium-oxide layer that is typically 20-40 angstroms thick [41]. It is the presence of this uniform chromium-oxide layer that imparts the enhanced corrosion resistance to 316L stainless steel. Although it is possible that the increased Cr_2O_3 formation at the surface does play a role in the observed decrease in the contact angles for all the test liquids, confirmation through physical analysis has not been previously reported. In particular, the contact angle for water showed a significant reduction in value, while diidomethane did not, suggesting a significant change in surface chemistry.

The results shown in Figure 21, which is a plot of the critical surface tension as a function of elongation and treatment, indicate that the electropolished and passivated surface (EPP) was the only surface that was within Baier's zone of biocompatibility for blood-contacting materials (Figure 6). All other surface treatments resulted in higher critical surface tensions, which suggests that they are relatively more likely to result in stent thrombogenicity. It is fortunate that the EPP process is the standard treatment most commonly used for the preparation of 316L stainless steel stents.

Also shown in Figure 21 is the effect of tensile elongation on the surface tension for each surface state. The results show that the effect of tensile elongation, although not as dramatic as for surface treatment, did result in differences to the measured γ_{crit}. In the case of the EP treated surface the effect of strain served to decrease γ_{crit} upon elongation to 15%. In the cases of the NT and PA surfaces the measured γ_{crit} increased slightly, while the γ_{crit} was unchanged following elongation to 15%. From a thermodynamic perspective, increased surface strain would be expected to result in an increased solid surface tension. However, the results for the surfaces tested here are not entirely consistent with that expectation. In plastic-strain, the dislocation density of the material undergoing strain increases. This increase in the dislocation density, and the resultant effect on γ_{crit}, is evidently not identical for all surface treatments. The EPP treatment resulted in a surface that was most resistant to strain effects. The results are encouraging from the standpoint that the stent implantation procedure does not necessarily predispose the high-strain areas of the stent to a greater risk of thrombogenicity, when the EP and EPP treatments are employed. One fact that should be pointed out is that the effect of

strain rate was not evaluated in this study. In clinical situations a stent reaches its nominal expansion diameter within approximately 30 seconds. The strain rate of 0.2 in/min used here was somewhat slower, and although it is expected that the final γ_{crit} values would be dependent only on the final strain level, any effect due to strain rate was not investigated.

6.3 Effect of Surface Treatment and Tensile Strain on Surface Roughness

Atomic Force Microscopy can be employed to image 3-dimensional topography on square areas down to the hundreds of angstroms range. The largest possible scan size, 100μ x 100μ, was used for this study to factor in the largest representation of the surface roughness. In some cases, i.e., the NT surface strained to 30%, the scale of the roughness would be large enough to warrant use of a profilometer; however, profilometer measurements do not provide a sufficient data for surface area differences calculations. Experimentally, it has been observed that as the scan area decreases, so does the computed roughness.

The topographical scan on the unstrained NT surface, from Table 17, shows that the standard 2B surface finish results in an extremely rough surface, as also reflected in the large surface area difference and peak-to-valley-distance in Table 18. Also evident in the scan is a surface that is composed of sharp streaks with very irregular heights. The effect of electropolishing only on 316L was to drastically reduce surface roughness over the as-received state, resulting in an optically "smooth" surface. However the EP surface is actually a "rough" surface relative to all other treatments tested, based on the average roughness results in Figure 23. The EP surface can either achieve a slightly improved

biocompatibility through elongation to small degrees of strain (< 15%), or, a more significant improvement through passivation.

In all cases, with the possible exception of the EPP surface, the effect of tensile elongation resulted in increased surface area. However, the peak-to-valley heights, as reflected in the R_{p-v} values, showed a general decrease with elongation. This shows a greater distortion of surface features, while at the same time, a leveling-off of the surface as a whole. This is visually reflected in the scans by the formation of areas of roughness within the surfaces.

To address the question of whether the γ_{crit} changes are a direct result of the surface roughness effects it is useful to examine the surfaces that performed the best, and worst, from a critical surface tension perspective; these would be the NT and EPP surfaces. The NT surface was in fact consistently the roughest, based on surface area differences. The NT surface also performed the worst from a critical surface tension perspective. The EPP demonstrated lower surface roughness and critical surface tension, relative to the other treatments. These results do indicate that a correlation does exist between roughness and surface tension, which is that as a surface becomes increasingly rough the corresponding critical surface tension increases (movement toward lower biocompatibility and higher thrombogenicity). However, the issues of whether roughness is the only cause for the observed differences in the surface tension measurements remains. The area where the surface roughness explanation seems to fall short is in explaining the differences in the Zisman plots of Figure 17 through Figure 20. The obvious shifts in the wetting patterns for the NT and PA, versus the EP and EPP surfaces,

indicates that a significant chemical change has occurred; however, other analysis such as Auger or Rutherford Back-Scattering (RBS) are needed to quantify factors such as oxide thickness and composition, in order to determine whether there are any changes in these characteristics as well.

Chapter 7

Conclusions

Based on the results of the critical surface tension measurements on 316L stainless steel, the surface treatment that consists of electropolishing and passivation results in the only surface that is within the previously established zone of biocompatibility for blood-contacting implants, such as stents. All other treatments resulted in critical surface tensions that were greater than the proposed range of biocompatibility. Yet, compared to the untreated 316L surface, all other treatments result in a more biocompatible surface.

The nature of the change in critical surface tension resulting from the various surface treatments is not entirely consistent with surface roughness effects, although the untreated surface did have the greatest roughness and surface area, which correlated with it also having the largest critical surface tension as well. Further experiments into determining the surface chemistry would need to be performed in order to determine whether the higher surface tension is resulting, for example, from strong polar interactions of the electropolished surface.

Measurement of the critical surface tension values following tensile elongation shows that the elongation does have an effect on critical surface tension, though not as significant as surface treatment did. In all cases, except for the electroplished surfaces (EP & EPP) the effect was to slightly increase the surface tension. However,

in the case of the standard preparation treatments (EP followed by PA) no significant change in thrombosis would be expected based on critical surface tension effects.

Chapter 8

Recommendations for Future Research

In general, additional work is needed in the areas of surface characterization to fully understand the dynamics at the biological and biomaterial interface, specifically, investigation that includes those properties listed in Table 2. Of particular importance is surface composition. The role of the oxide layer thickness and chemistry has not yet been investigated and correlated with wetting (surface energy). The use of Auger Electron Spectroscopy would serve to determine if oxide thickness, for example, is being affected by the surface treatments employed here. It has been shown here that surface morphology (roughness) alone cannot explain fully the results of the wetting analysis. However, in conjunction with surface morphology, the composition and thickness of the outer-most surface layer may better explain the observed results.

REFERENCES

1. Committee of the Working Group of Artherosclerosis, Report of the Working Group of Artherosclerosis of the National Heart, Lung, and Blood Institute. Vol 1 and 2, (Government Printing Office, Washington D.C. Dept. of Health Education and Welfare, no. 812034 and 82-2035, 1981).
2. A. Carrel, "*Results of the Permanent Intubation of the Thoracic Aorta*," Surg. Gyn. Obst. **15**, pp. 245-248 (1912).
3. C.T. Dotter, "*Transluminal Treatment of Artherosclerotic Obstruction: Description of a New Technique and Preliminary Report of its Application*," Circulation, **30**, pp. 654-660 (1964).
4. A.R. Gruntzig, "*Transluminal dilatation of Coronary Artery Stenosis*," Lancet, **4**, pp. 124-128 (1978).
5. U. Sigwart and G.I. Frank (ed's), Coronary Stents, (Springer-Verlag, New York, 1992), pp. 148-152.
6. C.T. Dotter, "*Transluminal Expandable Nitinol Coil Stent Grafting: Preliminary Report*," Radiology, **147**, pp. 259-260 (1983).
7. C.T. Dotter, "*Transluminally-placed Coiled End Arterial Tube Grafts*," Invet. Radiol. **4**, pp.329-332 (1969).
8. J.C. Palmaz, "*Expandable Intraluminal Vascular Graft: A Feasibility Study*," Surgery, **99**, pp. 199-205 (1986).
9. J. Sigwart, "Intravascular Stents to Prevent Occlusion and After Transluminal Angioplasty," Lancet, 316, p.701 (1987).
10. P.W. Serruys (ed.), Handbook of Coronary Stents, (Mosby, UK, 1997), pp. 50-54.
11. R.E. Baier, "*Selected Methods of Investigation for Blood-Contacting Surfaces*," in Blood in Contact with Natural and Artificial Surface, (Annals of the N.Y. Acad. Sci. vol. 516, New York, 1985), pp. 68-77.
12. U. Sigwart and G.I. Frank (ed's), Coronary Stents, (Springer-Verlag, New York, 1992), pp. 40-43.

13. P.S. Olson, "*Thrombus Formation in Stainless Steel Tubes as Vascular Implants in the Dog,*" Thrombosis Research, 4, no. 2, pp. 271-283 (1974).

14. H.M.M. Van Beuskom, P.W. Serruys and W.J. Van der Glessen, "*Coronary Stent Coatings,*" Coronary Artery Disease, **5**, pp. 590-598 (1994).

15. J.C. Palmaz, "*Intravascular Stents: Stent Interactions and Design Considerations,*" AJR, **160**, pp. 613-618 (1993).

16. J. Hirsh, "*Evolution of Thrombosis,*" in Blood in Contact with Natural and Artificial Surface, (Annals of the N.Y. Acad. Sci. 516, New York, 1987), pp. 586-604.

17. J.J. Goy and R. Eeckhout, "*Intracoronary Stenting,*" Lancet, **351**, pp. 223-226 (1998).

18. V.A. Depalma and R.E. Baier, "*Investigation of Three-Surface Properties of Several Metals and Their Relation to Blood Compatibility,*" J. Biomed Mater. Res. Symposium, **3**, pp.37-75 (1972).

19. R.E. Baier, "*Selected Methods of Investigation for Blood-Contacting Surfaces,*" in Blood in Contact with Natural and Artificial Surface, (Annals of the N.Y. Acad. Sci. vol. 516, New York, 1987), pp. 68-77.

20. C. Hehrlein, M. Zimmerman, J. Metz, W. Ensinger and W. Kubler, "*Influence of Surface Texture and Charge on the Biocompatibility of Endovascular Stents,*" Coronary Artery Disease, 6, pp. 581-586 (1995).

21. R.E. Baier, "*Surface Analysis*" in Handbook of BioMaterials Evaluation, (MacMillan Publishing Company, New York, 1986), pp. 97-108.

22. R.E. Baier, A.E. Meyer, J.R. Natiella, R.R. Natiella and J.M. Carter, "*Surface properties determine bioadhesive outcomes: Methods and results,*" J. Biomed. Mater. Res. **18**, pp. 337-355 (1984).

23. R.E. Baier, E.G. Shafrin and W.A. Zisman, " *Adhesion: Mechanisms that Assist or Impede it,*" Science, **162**, pp. 1360-1368 (1968).

24. B.D. Ratner, A.B. Johnston and T.J. Lenk, "*Biomaterial Surfaces,*" J. Biomed. Mat. Res. 21, pp. 59-90 (1987).

25. B. Kasemo and J. Lausmea, "*Biomaterial and Implant Surfaces: A Surface Science Approach,*" Int. J. Oral Maxillofac. Implants, 3, pp. 247-259 (1988).

26. C.J. Van Oss, Interfacial Forces in Aqueous Media, (Marcel Dekker, Inc., New York, 1994), pp. 65-66.

27. R. Good, "*Surface Free Energy of Solids and Liquids: Thermodynamics, Molecular Forces, and Structure,*" J. of Colloid and Interface. Science, **59**, pp. 398-419 (1977).

28. H.W. Fox and W.A. Zisman, "*The Spreading of Liquids on Low-Energy Surfaces. I. PTFE,*" J. Colloid Sci. pp. 514-531 (1950).

29. W.A. Zisman, "*Relation of the Equilibrium Contact Angle to Liquid and Solid Constitution,*" in Contact Angle, Wettability and Adhesion, (ACS, Washington, D.C., 1964), pp. 174-179.

30. F.M. Fowkes, "*Determination of Interfacial Tensions, Contact Angles, and Dispersion Forces in Surfaces by Assuming Additivity of Intermolecular Interactions,*" J. Phys. Chem. **66**, p. 382 (1962).

31. D.V. Kilpadi and J.E. Lemons, "*Surface Energy Characterization of Unalloyed Titanium Implants,*" J. BioMed. Mater. Res. **28**, pp. 1419-1425 (1994).

32. D.V. Kilpadi, T.J. Weimer and J.E. Lemons, " *Effect of Passivation and Dry-Heat Sterilization on Surface Energy and Topography of Unalloyed Titanium Implants,*" Colloids and Surfaces A: Physicochemical and Engineering Aspects, **135**, pp. 89-101 (1998).

33. R.E. Baier, "*The Role of Surface Energy in Thrombogenisis,*" Bull. N.Y. Acad. Med. **48**, pp. 257-272 (1972).

34. D.L. Coleman, D.E. Gregonis and J.D. Andrade, "*Blood-materials interactions: the minimum interfacial free energy amd the optimum polar/apolar ratio hypothesis,*" J. Biomed. Mater. Res. **16**, pp. 381-398 (1982).

35. E. Papirer, H. Balard, E. Brendle and J. Lignieres, "*Inverse Gas Chromatography Investigation of the Surface Characteristics of Stainless Steel Tubing,*" J. Adhesion Sci. Technol. **10**, pp. 1401-1411 (1996).

36. T. Amal, K. Hasouna, K. Nogi and K. Ogino, "*Effects of Surface Finish, Heat Treatment and Cold Working on the Wettability of Solid Copper by Liquid Tin,*" Trans. Jap. Inst. Metals, **10**, pp. 812-819 (1988).

37. R.N. Wenzel, "*Surface Roughness and Contact Angle,*" J. Phys. Colloid Chem. **53**, p.1466 (1949).

38. Standard Practice for Surface Preparation and Marking of Metallic Surgical Implants, ASTM F 86-91, Philadelphia, PA (1995).

39. Standard Practice for Tensile Testing, ASTM E8, Philadephia, PA (1995).

40. Standard Specification for 18Cr-12.5Ni-2.5Mo Stainless Steel for Cast and Solution-Annealed Surgical Implant Applications, ASTM F745-95, Philadelphia, PA (1995).

41. P. Lowery and D. Roll, "*Comparing the Characteristics of Surface-Passivated and Electropolished 316L Stainless Steel,*" Micro, Sep. pp. 43-49 (1998).

42. E. Nyilas, W.A. Morton, D.M. Lederman, T.H. Chiu and R.D. Cumming, "*Interdependence of Hemodynamic and Surface Parameters in Thrombosis,*" Trans. Amer. Soc. Artif. Int. Organs, **21**, pp. 55-70 (1975).

43. M. Triola, Elementary Statistics, 7th ed. (Addison-Wesley, New York, 1998), p. 247.

Appendix

Contact Angle Data

NT-0%

Ethylene Glycol

Ethylene Glycol

Ethylene Glycol

Diiodomethane

Diiodomethane

Diiodomethane

Formamide

Formamide

Formamide

Glycerol

Glycerol

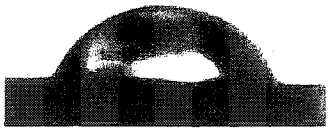

Glycerol

Water

Water

Water

NT-15%

Ethylene Glycol

Diiodomethane

Formamide

Glycerol

Water

Ethylene Glycol

Diiodomethane

Formamide

Glycerol

Water

Ethylene Glycol

Diiodomethane

Formamide

Glycerol

Water

NT-30%

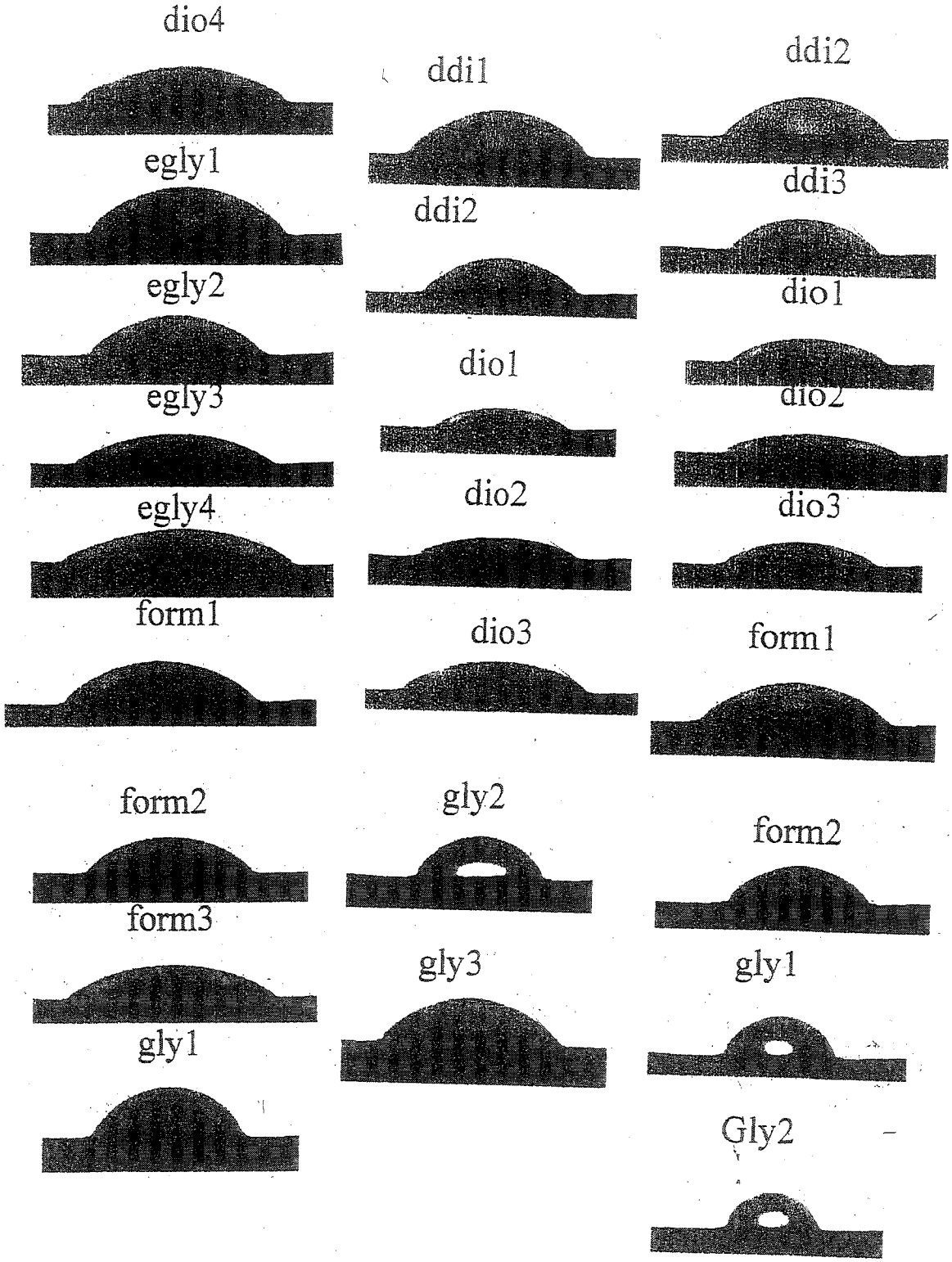
dio4
egly1
egly2
egly3
egly4
form1
form2
form3
gly1
ddi1
ddi2
dio1
dio2
dio3
gly2
gly3
ddi2
ddi3
dio1
dio2
dio3
form1
form2
gly1
Gly2

PA-0%

Cis-decalin

Ethylene Glycol

Glycerol

Ethylene Glycol

Diiodomethane

Water

Diiodomethane

Formamide

Water

Formamide

Glycerol

Glycerol

Water

Water

PA-15%

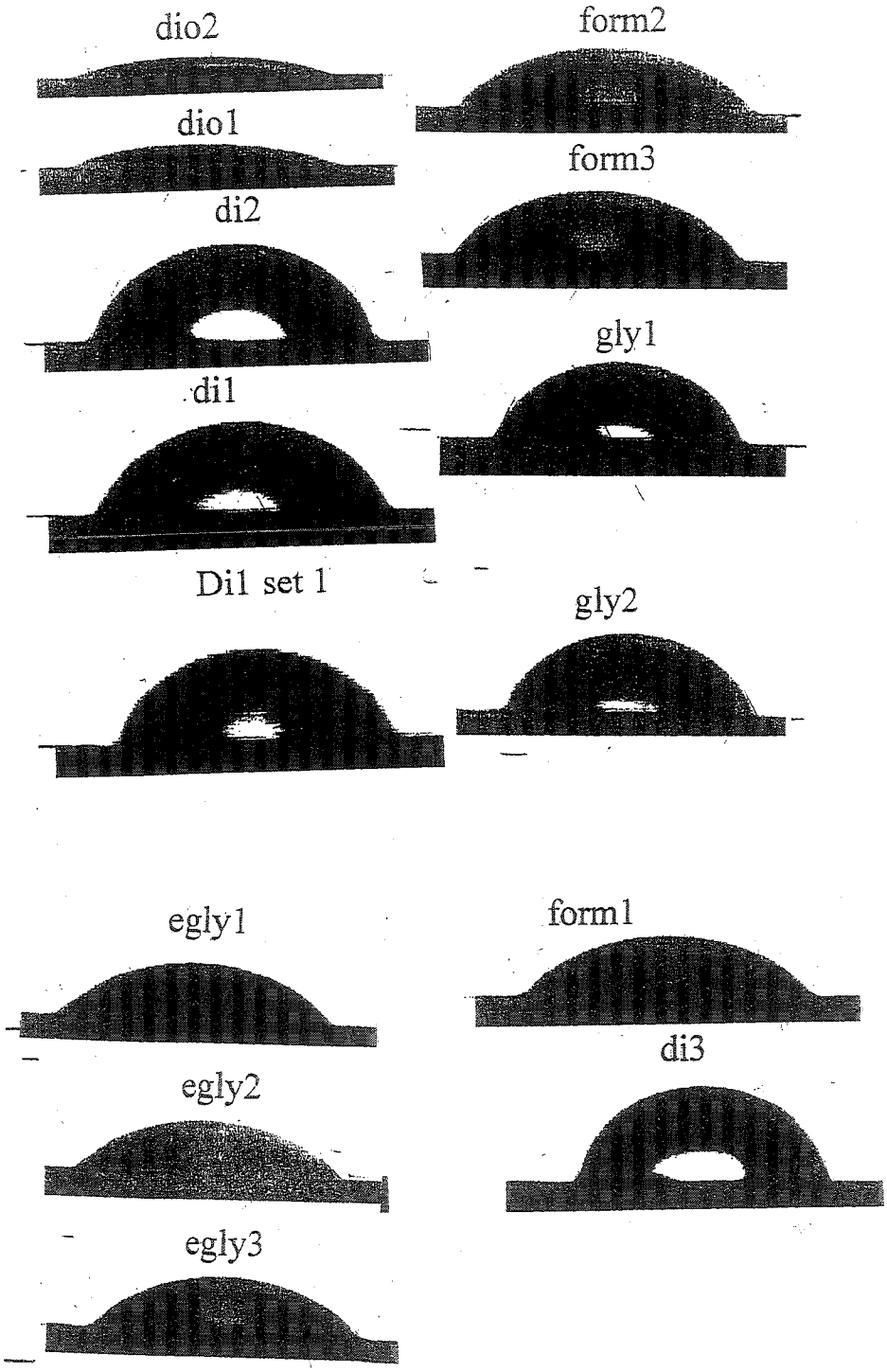
dio2
form2
dio1
form3
di2
gly1
di1
Di1 set 1
gly2
egly1
form1
di3
egly2
egly3

PA-30%

Ethylene Glycol

Diiodomethane

Formamide

Glycerol

Water

Ethylene Glycol

Diiodomethane

Formamide

Glycerol

Water

Ethylene Glycol

Diiodomethane

Formamide

Glycerol

Water

EP-0%

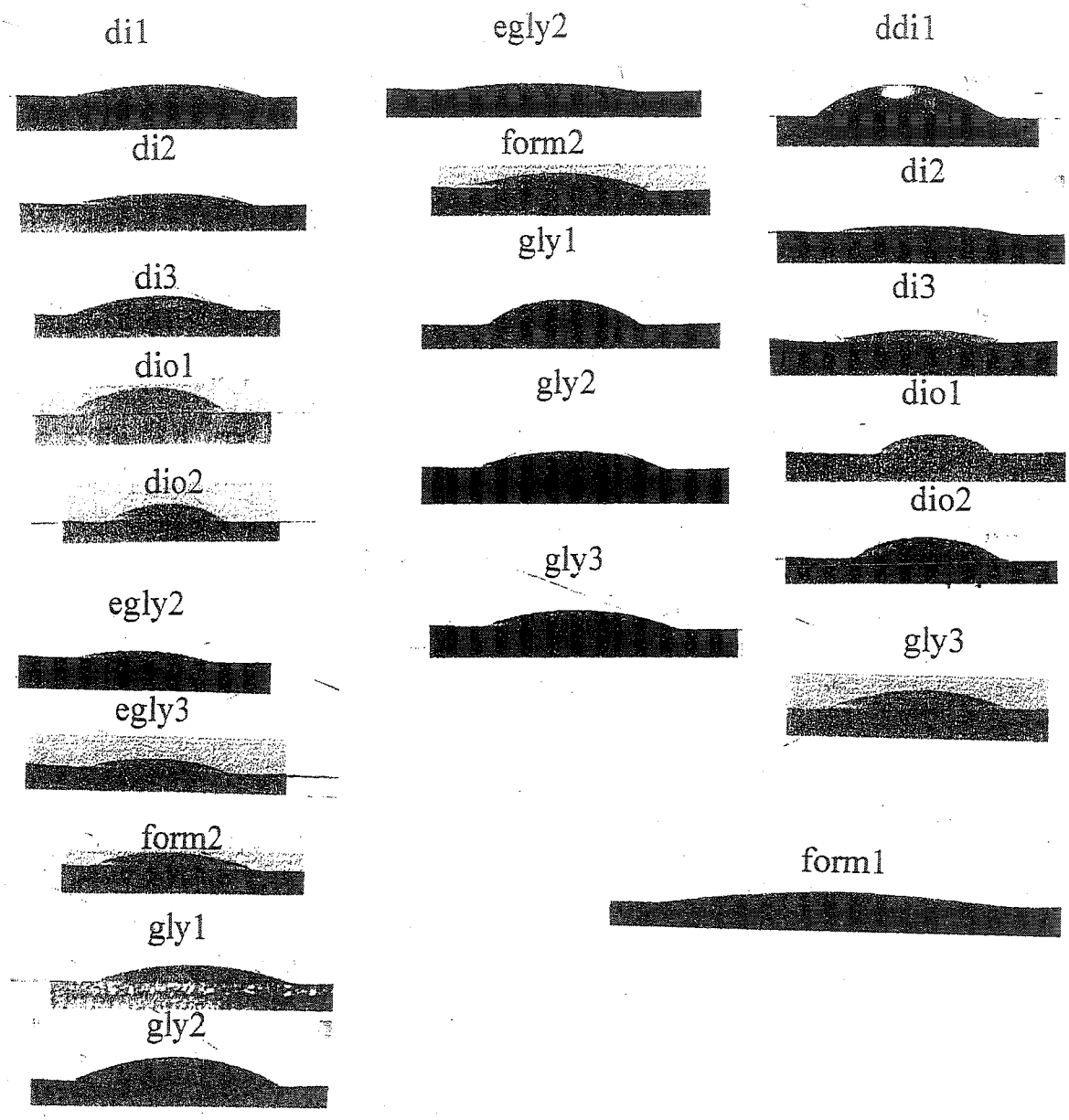
di1
di2
di3
dio1
dio2
egly2
egly3
form2
gly1
gly2
egly2
form2
gly1
gly2
gly3
ddi1
di2
di3
dio1
dio2
gly3
form1

EP-15%

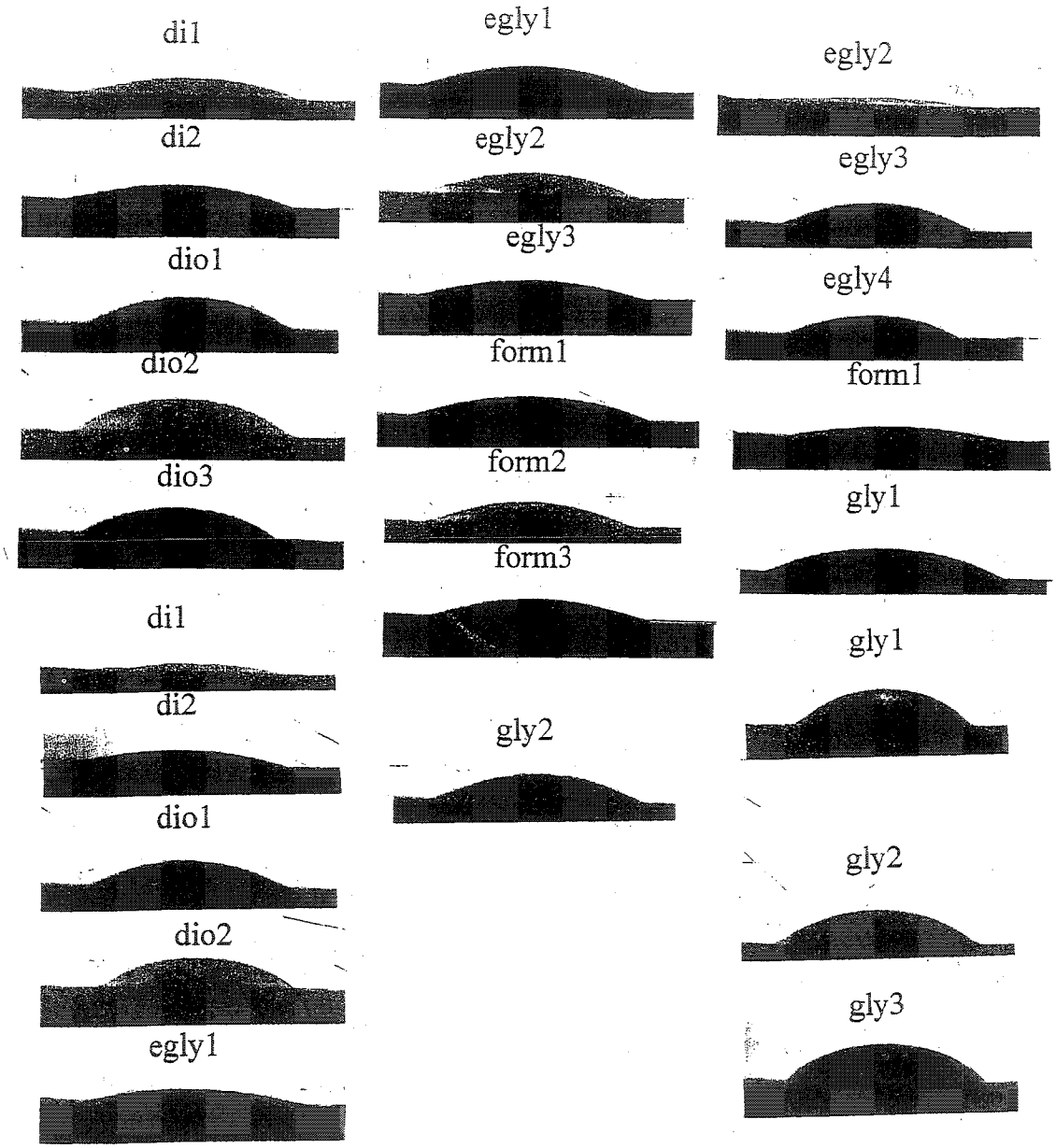
di1
di2
dio1
dio2
dio3
di1
di2
dio1
dio2
egly1
egly1
egly2
egly3
form1
form2
form3
gly2
egly2
egly3
egly4
form1
gly1
gly1
gly2
gly3

EP-30%

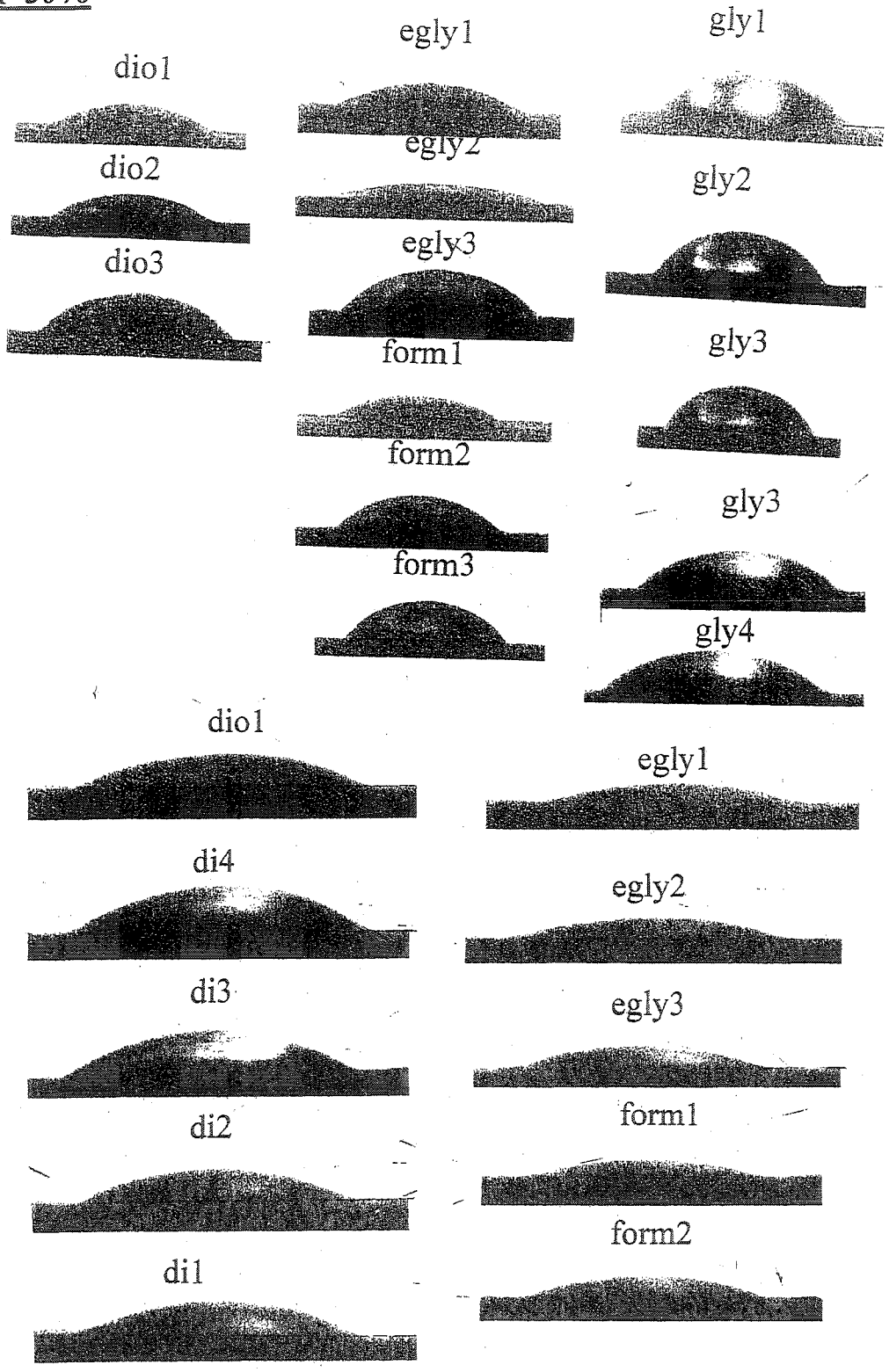
dio1
dio2
dio3
egly1
egly2
egly3
form1
form2
form3
gly1
gly2
gly3
gly3
gly4
dio1
di4
di3
di2
di1
egly1
egly2
egly3
form1
form2

EPP-0%

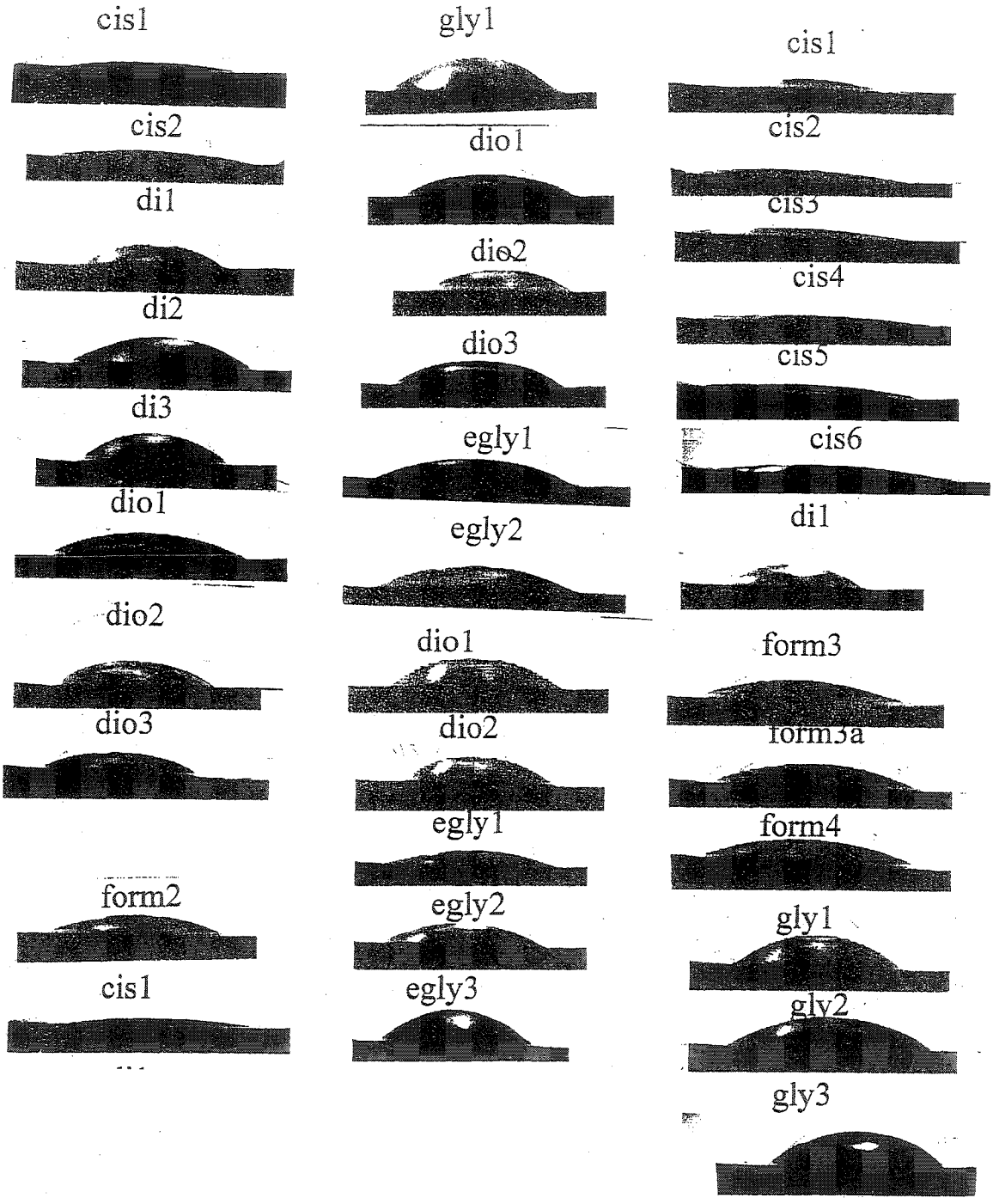
cis1
cis2
di1
di2
di3
dio1
dio2
dio3
form2
cis1
gly1
dio1
dio2
dio3
egly1
egly2
dio1
dio2
egly1
egly2
egly3
cis1
cis2
cis3
cis4
cis5
cis6
di1
form3
form3a
form4
gly1
gly2
gly3

EPP-15%

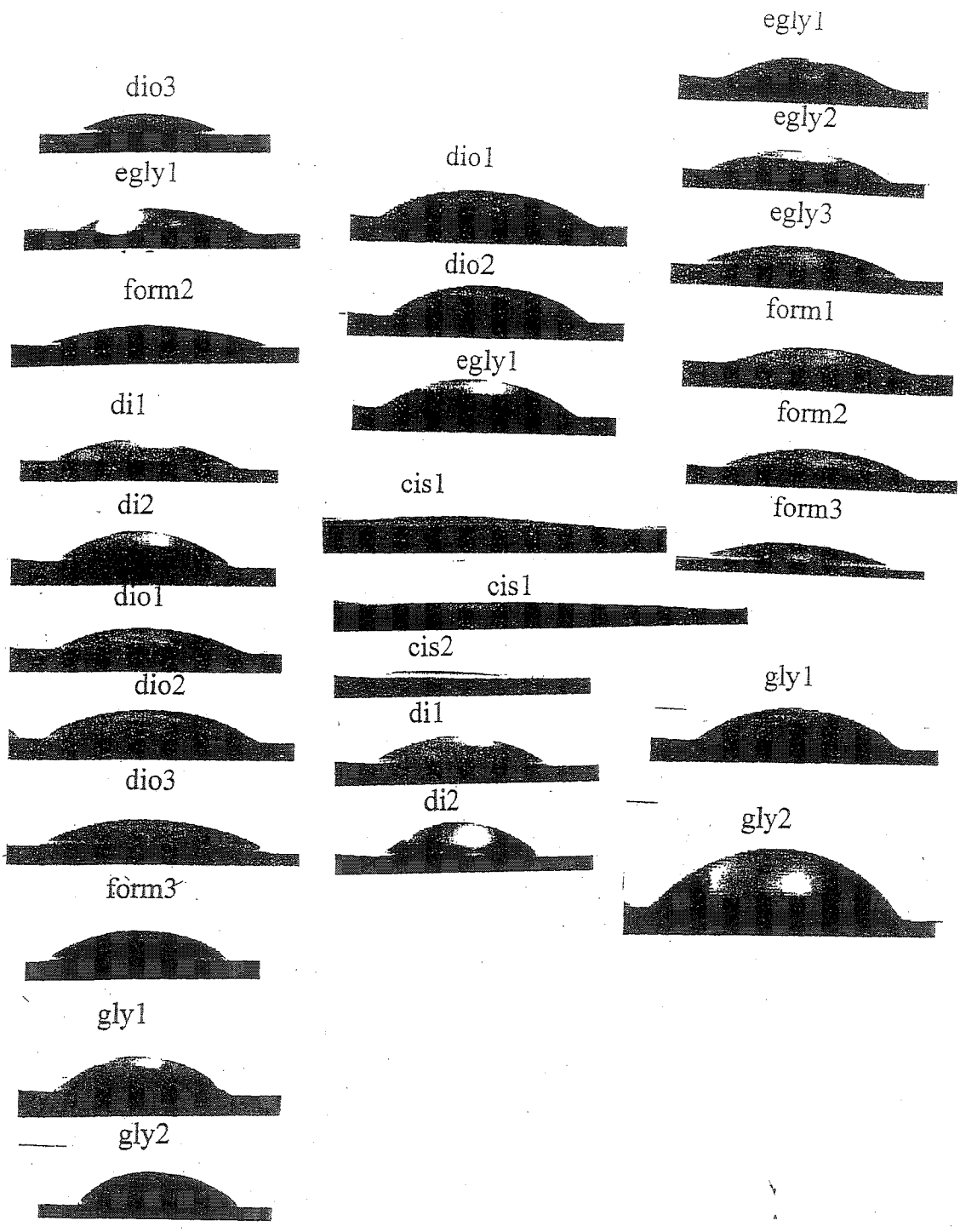
dio3
egly1
form2
di1
di2
dio1
dio2
dio3
form3
gly1
gly2
dio1
dio2
egly1
cis1
cis1
cis2
di1
di2
egly1
egly2
egly3
form1
form2
form3
gly1
gly2

EPP-30%

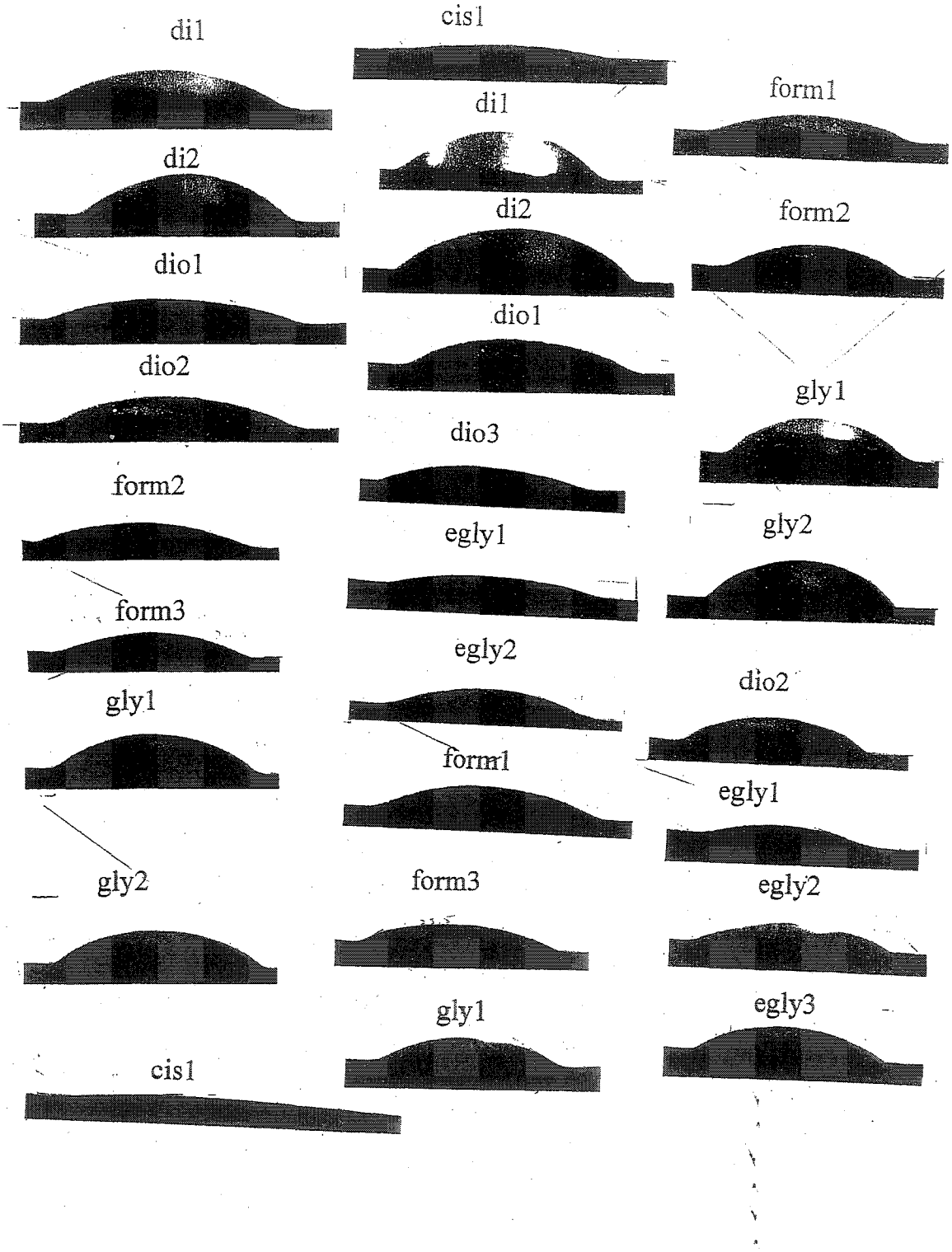
di1
di2
dio1
dio2
form2
form3
gly1
gly2
cis1
cis1
di1
di2
dio1
dio3
egly1
egly2
form1
form3
gly1
form1
form2
gly1
gly2
dio2
egly1
egly2
egly3